

Deployment Prior Injection for Run-time Calibratable Object Detection

Mo Zhou^{1,2} Yiding Yang² Haoxiang Li² Vishal M. Patel¹ Gang Hua²
¹Johns Hopkins University ²Wormpex AI Research

Abstract

With a strong alignment between the training and test distributions, object relation as a context prior facilitates object detection. Yet, it turns into a harmful but inevitable training set bias upon test distributions that shift differently across space and time. Nevertheless, the existing detectors cannot incorporate deployment context prior during the test phase without parameter update. Such kind of capability requires the model to explicitly learn disentangled representations with respect to context prior. To achieve this, we introduce an additional graph input to the detector, where the graph represents the deployment context prior, and its edge values represent object relations. Then, the detector behavior is trained to bound to the graph with a modified training objective. As a result, during the test phase, any suitable deployment context prior can be injected into the detector via graph edits, hence calibrating, or “re-biasing” the detector towards the given prior at run-time without parameter update. Even if the deployment prior is unknown, the detector can self-calibrate using deployment prior approximated using its own predictions. Comprehensive experimental results on the COCO dataset, as well as cross-dataset testing on the Objects365 dataset, demonstrate the effectiveness of the run-time calibratable detector.

1. Introduction

Object detection [17, 18, 37] aims to find and locate visual object instances (e.g., person, animal, vehicle, etc.) within digital images. It has a wide range of applications in areas such as autopilot, agriculture, and retail.

Typically, the training data for a detector contains dense objects of various kinds. Suppose the data distribution can be partly described as a graph structure as shown in Fig. 1 (a), where the nodes represent object classes, and the edges represent the object relations. In particular, we define “object relation” as the conditional probability¹ that one object class appears given the presence of another object class.

Object relation can be used as a context prior to facilitate

¹Conditional probability among object classes is asymmetric. Its explicit definition allows us to formulate expected model behavior intuitively.

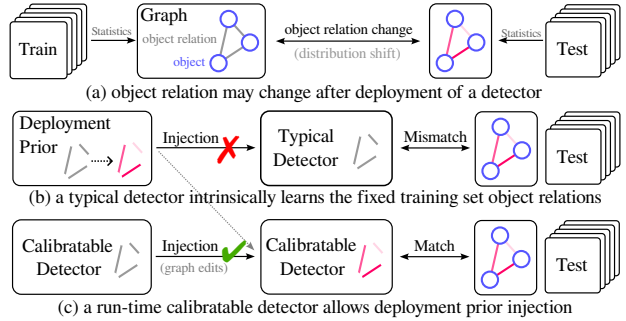


Figure 1. Calibratable Object Detector that allows Deployment Prior Injection at Run-time. The detector exposes a graph structure where the nodes are objects, while the edges are object relations. The model behavior is consistent with the graph structure, and hence deployment priors can be injected as graph edits.

object detection by assuming a match between the training and test data distributions. However, in the case of a test data distribution shift, the already learned contextual information from the training dataset will be regarded as a harmful bias.

Upon deployment, object detectors often encounter such test distribution changes due to variations in space (e.g., different geographical locations) and time (e.g., different seasons). Such changes, however, can sometimes be known in advance and regarded as “deployment prior”. For instance, Sprite may no longer co-occur with Coke after a shelf layout change in a retail store; bikes often co-occur with a person on the road but not in a shop. Expectedly, the detector will be influenced to some extent by the object relations learned from the training dataset, as demonstrated in Fig. 1 (b).

Take the COCO [28] dataset as an example. There is a notable relationship between the “person” and “baseball glove” classes, because $P(\text{person} \mid \text{baseball glove}) = 99.0\%$ in the training dataset. As a result, a typical object detector, such as DETR [3], implicitly learns the “baseball glove” representation with “person” information entangled, as shown by the gradient attribution of the “baseball glove” class in Fig. 2. Such entanglement is a context prior if it remains in the test distribution, or a bias if not. Nevertheless, it is permanently fixed once the training is finished, and obscure to revise.

The existing works for relation modeling are statically designed to either leverage [5, 27, 32] or mitigate (de-

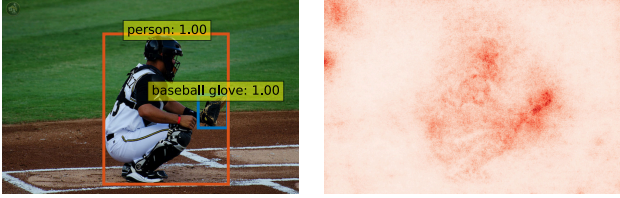


Figure 2. A detector [3] implicitly learns object relations via entangled representations. Since $P(\text{person} \mid \text{baseball glove}) = 99.0\%$ in the COCO training set, the gradient norm (shown on the right side) of the “baseball glove” show the shape of “person”. The gradient norm is visualized following the attribution method in [55].

bias) [40, 41, 48] the impact of context prior. But as long as the test distribution varies across space and time, these methods will frequently encounter distribution mismatch, and are not designed in a flexible way to adjust in run-time to either leverage or mitigate the prior. As straightforward countermeasures, fine-tuning or re-training with some new data upon every distribution change is an inefficient and endless loop, due to the non-static nature of the test distribution.

In contrast, we propose to learn a detector that can be calibrated to align the relation distribution at run-time without any parameter tuning, as shown in Fig. 1 (c). Specifically, a directed graph structure is exposed from the detector, where the nodes are object class embeddings, and the edges are weighted by the conditional probabilities (relations) among classes. The detector behavior is trained to be bounded by the graph structure. Thus, deployment priors can be injected into the detector as graph edits in edge weights, where a large weight means to leverage the contextual cue from another class, and a small weight means to mitigate such contextual cues. In this way, the detector can be calibrated at run-time to better match a shifted test data distribution.

A calibratable detector can be used as a drop-in replacement for a general detector. Even if the deployment prior is not available, the detector can be calibrated using its own prediction results through “self-calibration”. Thus, through either manually injected prior or self-calibration, the model can better match the shifted test distribution with object relation changes without fine-tuning, let alone re-training.

We evaluate the calibratable detector using different deployment priors. Notably, the more accurately the prior can describe the test data distribution shift, the better it performs. In the self-calibration scenario, the detector can improve object detection performance based on deployment prior approximated using its own predictions.

Contributions. To the best of our knowledge, this is the first work of a calibratable object detector, where deployment priors can be injected at run-time to adjust the detector behavior for shifted object relation distributions.

2. Related Works

Object Detection methods can be categorized into three groups: (1) two-stage detectors [17, 18, 37]; (2) one-stage detectors [29, 31, 36], and (3) DETR family [3, 14, 15, 26, 38, 53–55]. Specifically, DETR [3] eliminates manually designed components and employs the Transformer [42]. A deformable attention [55] is proposed to improve convergence speed and small object detection performance. The existing detectors tend to implicitly learn permanently fixed, data-specific, and non-calibratable object relations. Instead, we aim to make a detector run-time calibratable to adapt to distribution change without any parameter update.

Relation Modeling in object detection aims to build the relations between the objects in the image and facilitate object detection. Such context modeling is beneficial when the training and test distributions are similar [5, 10, 27, 32, 49, 50]. Based on granularity, they can be divided into three groups: (1) feature-level [7], (2) part-level [6], and (3) object-level [21]. For example, [21] uses the attention mechanism to build the relationship among detected proposals and refine their features. When the distributions mismatch, the relations learned by the model are turned into a harmful bias [40, 41, 48]. In contrast to modeling the relationship implicitly by the model, we build them explicitly from a global view. Specifically, a graph with editable edges is exposed to specify whether to leverage or mitigate these object relations, making the detector calibratable at run-time.

Meta Learning is widely explored in computer vision [13, 22, 25, 47, 52]. The goal of meta-learning is to train a model on a variety of tasks, such that it can better adapt to new tasks [13]. If we regard different deployment priors as “tasks”, the training of a calibratable detector aims to generalize against different priors by predicting a part of the model parameters, which will be detailed later.

Visual Prompting [1, 23] aims to learn a set of parameters at the input level, and Adapters [20, 33] learn to adjust intermediate representations, both for better adapting large-scale models for specific tasks. Although deployment prior resembles a kind of understandable prompt, our detector predicts a part of the model parameters according to it.

Graph knowledge including scene graph [4], knowledge graph [12], and even label graph [8] can aid object detection. Most of these graphs are used in a detector with hand-craft rules [12] or highly entangled modeling [8], and require external data. Conversely, our graph is merely a representation of the conditional probability statistics among classes, which does not rely on any external data than the detection dataset.

Despite slight resemblance to other topics including *domain adaptation* [2, 16, 46] and *test-time adaptation* [24, 34, 43–45], the proposed method is different. We focus on explicitly modeling the domain shift, which is the object relations in this paper, and build a framework to calibrate the test-time behavior of the detector without any back-propagation.

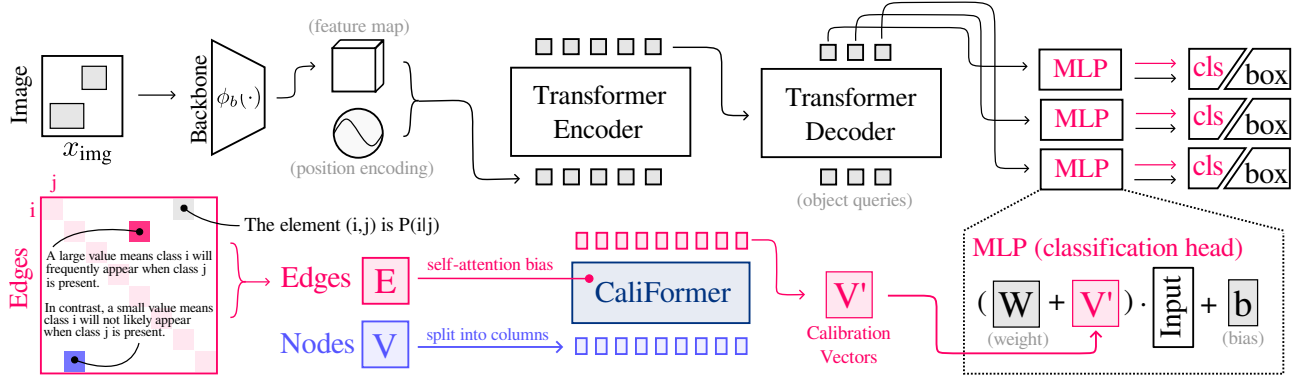


Figure 3. The architecture of our proposed run-time calibratable object detector (abbr., CaliDet). Injection of deployment prior is achieved by editing the edges E of the graph for the model. It can be used in DETR-like detectors [3, 54, 55], such as DINO [54]. This figure shows the CaliFormer for calibration vectors V' which is elaborated in Section 3.1. The other components in our model are elaborated in Section 3.2.

3. Calibratable Object Detector

The proposed method is built upon DINO [54], which casts object detection as set prediction [3, 55] using Transformer [42]. Given an object detection dataset with K object classes, comprising image-label pairs: (x_{img}, y) , where $x_{img} \in \mathbb{R}^{3 \times H_{img} \times W_{img}}$ is an RGB image, and y is a set containing N pairs of class and bounding box annotations $y = \{(c_i, b_i) | i = 1, \dots, N\}$. Denote $\phi_x(x_{img})$ as the backbone, which computes the feature map x of shape (C, H, W) . The Transformer takes x as input sequence and yields decoder outputs $\{h_m\}_{m=1}^M$ of length d for each of the M object queries. The h_m is used to predict scores and bounding box.

Beside the image, consider a graph $\langle V, E \rangle$ as an additional input. Specifically, the nodes $V \in \mathbb{R}^{d \times K}$ are per-class embeddings. The edge $E \in [0, 1]^{K \times K}$ is a conditional probability matrix for every pair of classes (object relations). The (i, j) -th element in E denotes the possibility that object class $i \in \{1, \dots, K\}$ appears given the presence of object class $j \in \{1, \dots, K\}$, *i.e.*, $P(i|j)$. The choice of conditional probability is based on the observed consistency between it and input pixel gradient attribution. The graph explicitly describes the relationship among classes.

Then, a calibratable object detector $f(x_{img}; V, E)$ predicts a set of label-box pairs with its behavior bound to V and E . Given the deployment prior $E \in [0, 1]^{K \times K}$, its injection is achieved as edge editing at run-time, which helps the detector better adapt to object relation changes. The closer the injected prior is to the real shifted relations, the better the detector performance is expected to be. The overview of the proposed framework can be found in Fig. 3. We abbreviate the proposed framework as ‘‘CaliDet’’.

As the calibration of V is conceptually incremental or transfer learning, which is beyond the scope of this paper, we specifically focus on the calibration of E (object relations). Therefore, we simplify the CaliDet notation as $f(x_{img}; E)$.

3.1. Calibratable Edges E for Node Interaction

The key idea for prior injection is to predict the class center shift based on $\langle V, E \rangle$. If we directly model the interactions among the nodes V with *e.g.*, Transformer, the model implicitly learns fixed relations, which is not calibratable at run-time. Instead, we model the node interactions using a modified encoder-only Transformer named ‘‘CaliFormer’’.

CaliFormer leverages E as a self-attention bias to interfere with the interactions among nodes V , and predicts the calibration vectors V' for class center shifts. In particular, we first convert the deployment prior into a difference matrix $\Delta E \triangleq E - E_0 \in [-0.5, 0.5]^{K \times K}$. The E_0 denotes the constant flat prior, for the case where there is no prior at all.

Subsequently, we modify the Transformer Encoder [42], where ΔE is used as a bias for the self-attention among V :

$$A = \text{softmax}\left(\frac{QK^T}{\sqrt{d_k}} + \Delta E^T\right)V, \quad (1)$$

where Q, K, V are the query, key, and value, respectively, as defined in [42]. This is a common [30, 51] modification.

Since ΔE interferes with the self-attention among V , it can be seen as a hint for increasing or decreasing the inclusion of cues of another class into the corresponding embedding. For example, denoting $\Delta P(i|j)$ as the (i, j) -th element of ΔE , a positive $\Delta P(i|j)$ informs the model to include more cues of class i into class j , or reduce the dependency of class j to class i by a negative $\Delta P(i|j)$. The case when $\Delta P(i|j) = 0$ means no deployment prior is provided. In this way, CaliFormer $g(\cdot)$ transduces the sequence of the columns of V into the per-class calibration vectors $V' \triangleq g(V, \Delta E)$. No position encoding is needed here, because the nodes V are permutation invariant.

After obtaining the calibration vectors V' , we incorporate them into the prediction heads of the object detector as the class center shifts, in order to adjust the detector behavior.

Prediction Head leverages a single linear layer for classification [3, 54, 55]. Let the linear layer be $\phi_c(h_m) = W^\top \cdot h_m + b$, where $W \in \mathbb{R}^{d \times K}$ is the weight, and $b \in \mathbb{R}^d$ is the bias. As the weights can be seen as object class centers [9], we add the calibration vectors V' , scaled by a constant factor ρ , to the weights to reflect the class center shifts:

$$\phi_c(h_m) = (W + \rho V')^\top \cdot h_m + b, \quad (2)$$

for dynamically adjusting the class centers based on the injected prior ΔE . The constant ρ is a scaling factor. The prediction head for bounding boxes is left unchanged.

3.2. Binding Detector Behavior to E

Assume the data distribution $\mathcal{X}(E)$ is parametrized by the edge E . Let E_0 be the flat prior², E_t be the statistics of training set, and E_v for validation set. E_x is the conditional probability matrix estimated³ using a single data point x . Similarly, E_b is estimated using a batch of data points. For example, $E_{b(1)} = E_x$ where the batch size is one.

Let $\mathcal{L}(\cdot)$ be the sum of classification loss and bounding box loss for a single training sample, a typical detector $f_{\theta^*}(\cdot)$ is trained to minimize the empirical risk on the training set:

$$\theta^* = \arg \min_{\theta} \mathbb{E}_{x \sim \mathcal{X}(E_t)} \{ \mathcal{L}[f_{\theta}(x)] \}. \quad (3)$$

In case of a distribution shift from $\mathcal{X}(E_t)$ to $\mathcal{X}(E_v)$, the model might perform slightly worse, as the model has implicitly learned the training set statistics E_t :

$$\mathbb{E}_{x \sim \mathcal{X}(E_v)} \{ \mathcal{L}[f_{\theta^*}(x)] \} \geq \mathbb{E}_{x \sim \mathcal{X}(E_t)} \{ \mathcal{L}[f_{\theta^*}(x)] \}. \quad (4)$$

Given the deployment prior, we use a calibratable detector $f_{\theta^\dagger}(x; E)$. The more accurate the given edge E is for describing the data, the more accurate the detector is expected to be. This can be expressed as the following inequality:

$$\begin{aligned} & \mathbb{E}_{x \sim \mathcal{X}(E_t)} \{ \mathcal{L}[f_{\theta^\dagger}(x; E_0)] \} \\ & \geq \mathbb{E}_{x \sim \mathcal{X}(E_t)} \{ \mathcal{L}[f_{\theta^\dagger}(x; E_t)] \} \\ & \geq \mathbb{E}_{x \sim \mathcal{X}(E_t)} \{ \mathcal{L}[f_{\theta^\dagger}(x; E_x)] \}. \end{aligned} \quad (5)$$

When a model can satisfy this inequality, it is expected to perform better on $\mathcal{X}(E_v)$ with $f_{\theta^\dagger}(x; E_v)$. Assuming that the model $f_{\theta^*}(\cdot)$ implicitly learns the E_t from $\mathcal{X}(E_t)$, then

$$\begin{aligned} \mathbb{E}_{x \sim \mathcal{X}(E_v)} \{ \mathcal{L}[f_{\theta^*}(x)] \} & \approx \mathbb{E}_{x \sim \mathcal{X}(E_v)} \{ \mathcal{L}[f_{\theta^\dagger}(x; E_t)] \} \\ & \geq \mathbb{E}_{x \sim \mathcal{X}(E_v)} \{ \mathcal{L}[f_{\theta^\dagger}(x; E_v)] \}. \end{aligned} \quad (6)$$

These require the detector behavior to be bound to E . While the deployment prior is injected into the model during training through the proposed architecture, the standard

²In E_0 , all off-diagonal values are 0.5. The diagonal values are 1.

³For each object class j present in the image, $P(i|j)$ is set to 1 when class i is present, or 0 when class i is absent. For each class j absent from the image, $P(i|j)$ will be inherited from flat prior E_0 as nothing is known.

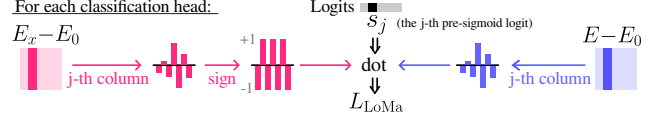


Figure 4. Demonstration of Logit Manipulation Loss (LoMa).

training loss is invariant to E , unable to guide the model to correctly utilize the information in E . So, we need to change the loss landscape with respect to E , by introducing an extra loss term to pose a higher penalty when the given E is more accurate, in order to implicitly enforce Eq. (5).

Logit Manipulation (LoMa). Denote s_j as pre-sigmoid logit for the class j at the classification head corresponding to decoder output h_m . Recall that the j -th column in $\Delta E = E - E_0$ denotes whether class j should depend more or less on each class i . Therefore, we use the mean value of the j -th column in $\text{sign}(E_x - E_0) \odot (E - E_0)$ to measure whether the arbitrary injected E is accurate or not, where “ \odot ” is element-wise product. Thus, the negative of this mean value is multiplied to s_j as the penalty for class j , encouraging s_j to be higher when E is accurate, or lower when inaccurate:

$$L_j = s_j \cdot \frac{1}{K} \sum_i [-\text{sign}(E_x - E_0)^{(i,j)} \cdot (E - E_0)^{(i,j)}]. \quad (7)$$

The term L_j is averaged over all classes as the LoMa loss for a single classification head: $L_{\text{LoMa}} = \gamma \sum_j L_j / K$, as shown in Fig. 4. The constant γ is a balancing hyper-parameter.

In this way, we reshape the loss landscape to peak at E_x where we expect better performance according to Eq. (5). And the loss is lower if we inject a misleading E .

Edge Sampling. A proper choice of E for training is vital for generalization against different E at run-time. To formulate the training objective, we first rewrite the original training objective in an equivalent double-expectation form:

$$\theta^* = \arg \min_{\theta} \mathbb{E}_{E \sim \delta(E_t)} \{ \mathbb{E}_{x \sim \mathcal{X}(E)} \{ \mathcal{L}[f_{\theta}(x)] \} \}, \quad (8)$$

with $\delta(E_t)$ denoting the Dirac function. It shows the training of θ^* is invariant to E . Replacing $\delta(E_t)$ with an edge sampling distribution \mathcal{E} will make the parameters optimized against varying E . Namely, the training of CaliDet aims to simultaneously generalize against different E and x :

$$\theta^\dagger = \arg \min_{\theta} \mathbb{E}_{E \sim \mathcal{E}} \{ \mathbb{E}_{x \sim \mathcal{X}(E_t)} \{ \mathcal{L}[f_{\theta}(x; E)] \} \}. \quad (9)$$

The dataset term is fixed at $\mathcal{X}(E_t)$ instead of $\mathcal{X}(E)$ because we only use one training dataset in practice.

Inspired by meta learning [13], we regard different E as different “meta tasks”. We empirically define the distribution \mathcal{E} by the following algorithm: (1) randomly select a prior from $\{E_x, E_b, E_t\}$ with equal probability; (2) generate a noise matrix from $\mathcal{N}(0, \sigma^2)$, and add it to the selected prior; (3) clip the prior to $[0, 1]$, and reset its diagonal to 1.

The E sampled from \mathcal{E} is used as an input to $f_{\theta^\dagger}(\cdot; \cdot)$ for training, and re-calculated for every mini-batch. The Gaussian noise facilitates generalization by covering more different E , and prevent overfitting at E_x , E_b and E_t .

3.3. Inference and Run-time Calibration

During the inference stage, deployment prior is injected to the model via the input E as $f_{\theta^\dagger}(x; E)$. When there is no prior, we use $E = E_t$ (training set statistics) as the default. Given an arbitrary set of x , the result of $f_{\theta^\dagger}(x; E)$ varies according to the given E . The more accurately that E describes the distribution from which x is drawn, the more accurate the result should be. Since the injection process is merely changing the $K \times K$ input matrix E , while leaving model parameters intact, it is called “run-time” calibration.

Self-Calibration. In practice, the deployment prior is not always available. In the worst case, the object relations in the new distribution are completely unknown. This does not mean the detector is limited by the assumption that the deployment prior is available. In contrast, the detector can still automatically find an approximate prior to calibrate itself. This algorithm is summarized in Algo. 1.

Given an arbitrary set of sample images X , we first initialize the self-calibrated edge E_c as the default prior E_t , because the object relation shift with respect to E_t in the underlying distribution of X is unknown.

Next, we forward the model $f_{\theta^\dagger}(x; E_c)$ on the given set X , and calculate the conditional probability matrix E_i purely based on the model predictions. Before we move E_c towards E_i with a step size η , it must be pointed out that an imperfect detector $f_{\theta^\dagger}(x; E_c)$ will expectedly produce false predictions, which could mislead the detector.

Hence, a weight matrix $Z \in \mathbb{R}^{K \times K}$ is introduced. We first calculate a vector $z \in \mathbb{R}^{1 \times K}$ corresponding to every $x \in X$, where the i -th element of z is the maximum confidence score among the predictions for class i , or 0 when class i is not predicted from x . Then, we figure out the average z , and repeat it to satisfy the shape of Z . As a result, the E_c update is mainly guided by confident predictions, lest the detector be quickly misled by its own faulty predictions. We iteratively update E_c with a frozen CaliDet when no prior is available. The clip operation ensures that E_c remains a matrix with valid conditional probability values.

In this way, a frozen model can still obtain a performance gain upon an arbitrary test distribution shift for “free” (i.e., without any parameter update or data annotation).

4. Experiments

In this paper, we aim to endow a detector with the run-time calibration capability without sacrificing the default AP (no injection) compared to the baseline detector. The experiments are conducted with eight NVIDIA RTX A5000 GPUs. Our code is based on PyTorch [35] and DINO [54].

Algorithm 1 Self-Calibration with E_c

Input: Arbitrary set of samples X and step size η .
Output: Self-calibrated edge $E_c \in [0, 1]^{K \times K}$.

```

1:  $E_c \leftarrow E_t$             $\triangleright$  Initialize  $E_c$  as the default prior
2: for  $i \leftarrow 1, 2, \dots$ , MaxIteration do
3:    $E_i \leftarrow \text{Statistics}\{f_{\theta^\dagger}(x; E_c) \text{ for all } x \in X\}$ 
4:    $Z \leftarrow \text{Repeat}(\text{Mean}\{z \text{ for all } x \in X\})$ 
5:    $E_c \leftarrow \text{Clip}\{E_c + \eta Z \cdot (E_i - E_c), [0, 1]^{K \times K}\}$ 
6: end for

```

Dataset. To validate our method, we conduct experiments on the COCO 2017 dataset [28], following [3, 54, 55]. It contains 118K training images and 5K validation images.

Baseline. We adopt DINO [54] (4 scales, ResNet-50 [19] backbone, 12 epochs) as the not calibratable baseline. Unless explicitly mentioned, we retain all overlapping model details. Note, the proposed method is not specific to DINO. See supplementary for experiments on D-DETR [55].

Training. To accelerate the training process, we initialize our model from the officially pre-trained DINO [54]. The learning rate for the pre-trained parts is decayed by 0.1 at the beginning. The training scheme is 6 epochs with learning rate decay after 5 epochs, in order to roughly align our model’s default AP (i.e., $E = E_t$) with the baseline AP.

Tunables. The embedding dimension $d = 256$ for V is also the Transformer dimension. The nodes V are initialized with $\mathcal{N}(0, 0.01^2)$ following [9]. The CaliFormer consists of 3 layers of Transformer Encoder with the attention bias described in Sec. 3.1. We set the scaling factor of V' as $\rho = 0.2$; the balancing parameter $\gamma = 20$ for L_{LoMa} ; the Gaussian variance as $\sigma^2 = 0.16^2$ for \mathcal{E} ; the step size $\eta = 4.0$ for self-calibration. We use a mini-batch of size 2 following [54].

4.1. Evaluation Protocol for Calibratable Detector

Standard Evaluation (Sec. 4.2). To verify if the proposed method can adapt to distribution shifts at run-time, it is evaluated against different priors, ranging from inaccurate ones to accurate ones: $\overline{E_x}$, E_0 , E_t , E_v , E_b , E_x . The $\overline{E_x}$ is the result of flipping 0 and 1 in E_x except for the diagonal, and hence is the most misleading one. For the validation dataset $\mathcal{X}(E_v)$, we expect the Average Precision (AP) [3, 55] to be higher if the provided E is accurate, or lower if misleading. The E_t is regarded as the default deployment prior. And the AP when injecting E_x can provide an empirical performance upper bound with prior injection according to Eq. (5). If the model performance follows the expected order, it means the model has generalized for different edges covered by \mathcal{E} .

Subset Evaluation (Sec. 4.3). In well-controlled datasets, the test distribution may not significantly deviate from E_t . As $E_v \approx E_t$, the performance gain by injecting E_v may be negligible. To simulate some shifts from E_v , we randomly segment the validation set into a series of equal-sized

Method	Injection	Standard COCO Metrics					
		AP	AP ₅₀	AP ₇₅	AP _S	AP _M	AP _L
DINO [54]	-	49.07	66.72	53.57	32.67	52.36	63.04
CaliDet (DINO)	\bar{E}_x	35.83	46.48	39.10	18.14	38.07	53.24
	E_0	47.97	64.50	52.37	30.79	51.65	62.49
	E_t	49.27	66.73	53.80	32.75	52.57	63.50
	E_v	49.30	66.77	53.84	32.77	52.58	63.53
	E_b	51.69	70.62	56.48	35.82	55.08	65.29
	E_x	51.94	70.92	56.69	36.10	55.27	65.76

Table 1. Standard COCO Evaluation Results. The AP given the default deployment prior E_t is close to that of the baseline method. Compared to E_t , the less accurate edges \bar{E}_x and E_0 lead to lower performance, while more accurate edges such as E_x lead to higher performance. Note, as shown in Fig. 5, the difference between E_v and E_t is marginal to make a larger difference in AP. Likewise, the difference between E_b and E_x is also small because the mini-batch size is 2 for DINO. Namely $E_{b(2)} \approx E_x$.

non-overlapping subsets, and inject the corresponding subset statistics E_b . Note, in this case, E_b is still a random matrix centered at E_v , but along with a notable variance. The performance averaged over subsets is expected to be higher with E_b compared to E_t . Note, according to the Law of Large Numbers, the conditional probability statistics calculated from a larger subset will be more approximate to E_v . Thus, very large subsets are not necessary for subset evaluation.

Self-Calibration (Sec. 4.4). In the subset evaluation, we use the subset statistics E_b as the deployment prior. However, those statistics are not always available in practice as the statistics rely on annotations. Thus, we use the model’s own predictions to calibrate itself on random subsets, and show the performance curves during the process of Algo. 1.

4.2. Standard Evaluation w/ Different Priors

As a prerequisite for a valid calibratable detector, its detection performance by the standard COCO metrics should be at least on par with the baseline. Thus, we compare the baseline model to our model with the default deployment prior in these metrics in Tab. 1. Meanwhile, we inject different priors to verify whether the model can leverage the injected prior. Note, the injection process only changes the input edge E .

The baseline achieves 49.07 overall AP, while our model achieves an on-par performance 49.27 with the default prior E_t inherited from the training set. When we provide the flat prior E_0 , which is less accurate than E_t , and represents the case when there is no prior knowledge at all, the model performs slightly worse by 1.30 AP. If we provide an even worse prior \bar{E}_x to intentionally “mislead” the model, the performance further drops to 35.83.

If we provide the E_v as the prior, the performance slightly improves compared to the E_t case. This is because, on the well-controlled COCO dataset, the difference between E_t

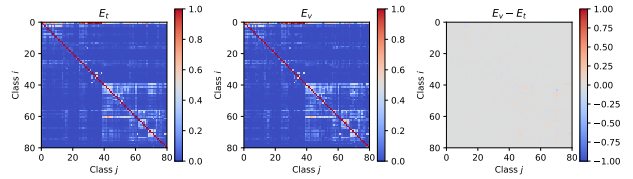


Figure 5. Visualization of E_t , E_v , and $E_v - E_t$. The mean absolute error between the two matrices is $\epsilon = \sum \text{abs}(E_v - E_t) / K^2 = 0.008$. The 0-th, 50-th, 90-th, 97-th, 100-th percentile values of $\text{abs}(E_v - E_t)$ are 0.0, 0.003, 0.021, 0.044, 0.272, respectively.

and E_v is too marginal to make a larger difference in AP, as shown in Fig. 5. Notably, the difference between E_v and E_t is even smaller than the Gaussian noise used for the edge sampling during the training process. This observation is exactly our motivation for the subset evaluations with a much larger simulated relation shift.

Conversely, if we provide a more accurate prior, such as the mini-batch prior E_b and the per-sample prior E_x (most accurate), the performance will be improved to 51.69 and 51.94. Note, the difference between E_b and E_x is small because the mini-batch size is 2 for DINO. Namely $E_{b(2)} \approx E_x$ in this case. Although it may be impossible to obtain E_x upon deployment, the corresponding performance can be regarded as the empirical upper bound of the performance gain through calibration. The experiments demonstrate that the detector behavior is effectively bound to E .

In summary, the experiments in Tab. 1 demonstrate that: (1) our method does not sacrifice performance compared to the baseline method, unless we intentionally mislead the model with a wrong prior; (2) All the AP metrics follow the expected order, that a more accurate edge leads to a higher AP, while a less accurate edge leads to a lower AP. This reflects our expectation in Eq. (5) and Eq. (6). Empirically, this is a sanity check when tuning the hyper-parameters when adopting CaliDet to a different baseline detector.

4.3. Subset Evaluation (Simulated Shifts)

In the previous subsection, we note the difference between E_v and E_t is marginal on COCO, a well-controlled dataset. This does not lead to a clear difference when E_v is injected compared to the default prior, *i.e.*, E_t . Thus, we split the validation set into subsets with varying sizes to simulate the distribution shift, and report the metrics averaged over all subsets, as shown in Tab. 2. Note, the injection only changes the input edge E , with model parameters being frozen.

With a small subset size (*e.g.*, 8), the corresponding subset statistics $E_{b(8)}$ will clearly deviate from E_t , as suggested by its mean absolute error ϵ with respect to E_t . This can lead to a clear performance gain when we inject the corresponding priors. For instance, the AP increases from 62.93 (E_t) to 63.15 with the subset size 8 and the subset statistics $E_{b(8)}$ as

Subset Size	Injection	ϵ	Metrics Averaged over COCO Subsets					
			AP	AP ₅₀	AP ₇₅	AP _S	AP _M	AP _L
8	E_t	0	62.93	79.69	67.56	45.90	66.41	79.77
	$E_b(8)$	0.331	63.15	80.01	67.76	46.10	66.66	79.87 (+ 0.22) (+ 0.32) (+ 0.20) (+ 0.20) (+ 0.25) (+ 0.10)
16	E_t	0	61.06	77.63	65.52	44.40	64.65	78.21
	$E_b(16)$	0.276	61.31	77.96	65.77	44.56	64.83	78.44 (+ 0.25) (+ 0.33) (+ 0.25) (+ 0.16) (+ 0.18) (+ 0.23)
32	E_t	0	59.74	76.05	64.17	42.70	63.16	76.85
	$E_b(32)$	0.202	60.00	76.39	64.44	42.82	63.43	77.00 (+ 0.26) (+ 0.34) (+ 0.17) (+ 0.12) (+ 0.27) (+ 0.15)
64	E_t	0	57.89	74.21	62.41	40.94	61.69	75.07
	$E_b(64)$	0.122	58.13	74.54	62.67	41.07	61.96	75.20 (+ 0.24) (+ 0.33) (+ 0.26) (+ 0.13) (+ 0.27) (+ 0.13)
128	E_t	0	55.74	72.16	60.32	39.17	60.04	72.89
	$E_b(128)$	0.062	55.89	72.35	60.47	39.25	60.12	72.98 (+ 0.15) (+ 0.19) (+ 0.15) (+ 0.08) (+ 0.08) (+ 0.09)
256	E_t	0	53.67	70.33	58.26	37.62	57.77	71.09
	$E_b(256)$	0.034	53.82	70.50	58.44	37.70	57.94	71.14 (+ 0.15) (+ 0.17) (+ 0.18) (+ 0.08) (+ 0.17) (+ 0.05)

Table 2. Subset Evaluation with Varying Subset Size. We split the validation datasets into subsets with varying sizes, and report the metrics averaged over all subsets of the respective sizes. CaliDet shows a “free” (*i.e.*, without any parameter update) performance gain as long as a more accurate prior than E_t is provided.

the injected prior. The results for the other subset sizes also suggest a performance gain compared to E_t , as long as the corresponding E_b clearly differs from E_t .

As discussed in Sec. 4.1, a larger subset size will make the subset statistics E_b closer to E_v , while $E_v \approx E_t$. When the subset size is 256, the injection of $E_b(256)$ leads to a less notable difference in performance, because it is very close to E_v as $\epsilon = 0.034$. We refrain from experimenting on larger subsets because they do not simulate clear distribution shifts.

In summary, the subset evaluation for simulating distribution shifts by relation change demonstrates the effectiveness of the proposed method. As long as the prior is more accurate than E_t , a consistent performance gain is expected for “free”, *i.e.*, with merely changes in the input matrix E while keeping the whole model frozen. Thus, CaliDet is effective.

4.4. Self-Calibration Evaluation

In practice, the deployment prior is not always available. Thanks to the statistically meaningful definition of object relations, the CaliDet can be designed to calibrate itself using its own prediction results following Algo. 1. Specifically, we sample subsets of varying sizes from COCO validation set. The subsets of each size sum up to 1024 samples. During self-calibration, each individual subset is regarded as the set of images samples X used Algo. 1, and the model is frozen.

The self-calibration results for different subset sizes can be found in Fig. 6, 7, 8, 9, 10, 11. Besides the AP metrics,

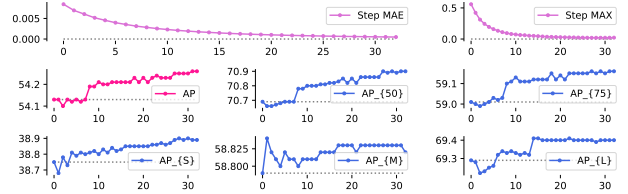


Figure 6. Self Calibration Results with Subset Size 256.

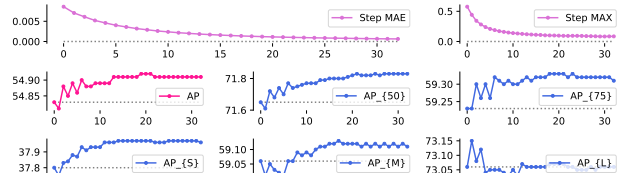


Figure 7. Self Calibration Results with Subset Size 128.

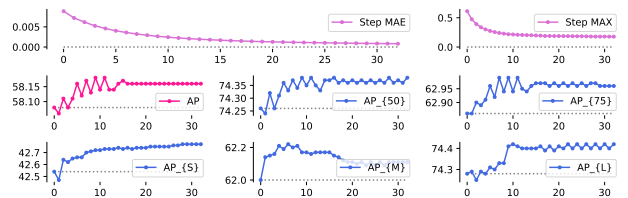


Figure 8. Self Calibration Results with Subset Size 64.

we track two additional quantities: (1) “Step MAE”: the step-wise mean absolute error of E_c ; (2) “Step MAX”: the maximum absolute value in the update step of E_c . The two values indicate whether the algorithm is converging.

Take the subsets with size 256. The results are shown in Fig. 6. An improvement in the overall AP can be seen along the self-calibration process. The process is converging since the Step MAX will almost decay to zero in the end.

For subsets of smaller sizes, the self-calibration process will also lead to an improvement in the overall AP without any back-propagation, as shown in Fig. 7, 8, 9, 10, 11. Differently, while the Step MAE is always decreasing for any subset size, the Step MAX will saturate at a larger value on smaller subsets. This is because smaller subsets cannot provide a relatively stable statistics, and many conditional probability values in E_c will fluctuate during the self-calibration process. Meanwhile, the AP curves will also fluctuate, especially on the smallest subset, as shown in Fig. 11.

Convergence is important. When the model is deployed, it is not necessary to self-calibrate on a fixed set of images, resulting in some inference overhead. Instead, the method can use running statistics from the past predictions to gradually calibrate itself towards the underlying test distribution.

Based on these results, CaliDet can effectively calibrate itself with its own predictions. In practice, more samples will make the process more smooth in terms of AP curves.

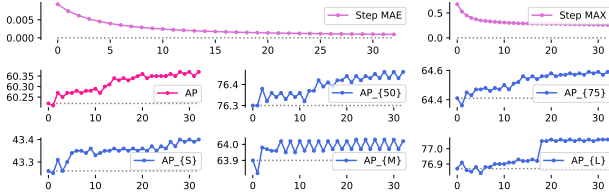


Figure 9. Self Calibration Results with Subset Size 32.

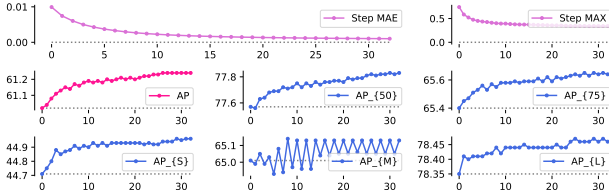


Figure 10. Self Calibration Results with Subset Size 16.

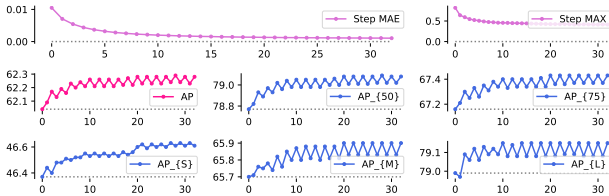


Figure 11. Self Calibration Results with Subset Size 8.

5. Ablation Studies & Discussions

In this section, we review the contribution of each component in the proposed method, and discuss the limitations. In particular, CaliDet comprises three main components in its implementation: (1) CaliFormer; (2) Logit Manipulation loss, and (3) the edge sampling distribution \mathcal{E} .

CaliFormer models the interaction among nodes V , and provides the calibration vectors V' . It is the only entry point for prior injection as described in Eq. (1). Thus, replacing this component with standard Transformer will directly lead to a not calibratable model. The scaling factor in Eq. (2) is empirically set as $\rho = 0.2$ for best performance. Setting it to a larger value leads to a lower AP, while a smaller ρ value leads to a weaker effect with different deployment priors.

Logit Manipulation. This loss guides the model on the correct usage of the information in the columns of E . Removing this loss will lead to poor generalization and make the effect of calibration almost vanish. Namely the model without LoMa does not satisfy the expectation that the $AP(E_v)$ should be at least slightly greater than $AP(E_t)$. This loss term has a hyper-parameter γ to balance its magnitude with the other detection loss terms. Making γ larger means to encourage the model to follow the given E to a higher extent, but will meanwhile distract the model from the detection loss and lead to a worse AP. We omit the corresponding experimental results for brevity.

Module	Backbone	Detection Transformer	CaliFormer
Time (Ratio)	17.10 ± 2.88 (25.8%)	47.86 ± 7.06 (72.2%)	1.37 ± 0.30 (2.0%)

Table 3. Inference Time per Image. The unit is millisecond.

Edge Sampling. This provides the model with different E during the training process for generalization to the arbitrary E provided at run-time, as described in Sec. 3.2. For each mini-batch, we randomly choose a prior from $\{E_x, E_b, E_t\}$, namely the statistics for a single sample, the mini-batch, and the whole training set. According to our observation, the diversity of edges is very important for the model’s generalization against different priors. For instance, using only E_t or E_x leads to overfitting at E_t or E_x , and hence performs poorly at other different edges.

Besides, a Gaussian noise is applied to the randomly chosen edge. It increases the area covered by \mathcal{E} during the training process, and helps the model better generalize against different E . For instance, the $AP(E_v)$ is lower than $AP(E_t)$ without the noise, which is undesired. If its variance is excessively large, the model will learn to discard the too noisy injection and end up with a weak effect of calibration.

Overhead. The inference time cost with an NVIDIA RTX A5000 GPU is shown in Tab. 3. Compared to the backbone and the detection transformer, our method only introduces a negligible computational overhead through CaliFormer. In practice, since it is not necessary to update the deployment prior upon every single forward pass, the calibration vectors V' can be cached until the deployment prior update. In this way, the overhead introduced by our method is further reduced based on the frequency of deployment prior update.

Limitations. Deployment prior is the relation among different object classes. For datasets with a small average number of objects per image (e.g., Pascal VOC [11]), the performance gain of prior injection could be marginal because the leverageable object relation is relatively scarce.

Future Work. The core idea behind CaliDet can be interpreted differently. If some statistical properties of the test distribution can be characterized, we may be able to bind the model behavior with such properties as an input, and calibrate the model at the run-time for distribution shift.

Supplementary document contains elaborations on how to calculate different edges, more technical details, experiments on D-DETR [55], as well as evaluations on Objects365 [39] dataset with the model trained on COCO.

6. Conclusions

With a run-time calibratable object detector, the deployment prior can be injected to adapt it to shifted object relation distribution without any parameter update. The more accurate the injected prior is, the better it performs. When no deployment prior is available, the model can still leverage its own prediction results for self-calibration.

References

[1] Hyojin Bahng, Ali Jahanian, Swami Sankaranarayanan, and Phillip Isola. Exploring visual prompts for adapting large-scale models. *arXiv preprint arXiv:2203.17274*, 1(3):4, 2022. 2

[2] Qi Cai, Yingwei Pan, Chong-Wah Ngo, Xinmei Tian, Lingyu Duan, and Ting Yao. Exploring object relation in mean teacher for cross-domain detection. In *Proceedings of the IEEE/CVF Conference on Computer Vision and Pattern Recognition*, pages 11457–11466, 2019. 2

[3] Nicolas Carion, Francisco Massa, Gabriel Synnaeve, Nicolas Usunier, Alexander Kirillov, and Sergey Zagoruyko. End-to-end object detection with transformers. In *European conference on computer vision*, pages 213–229. Springer, 2020. 1, 2, 3, 4, 5

[4] Xiaojun Chang, Pengzhen Ren, Pengfei Xu, Zhihui Li, Xiaojiang Chen, and Alexander G. Hauptmann. A comprehensive survey of scene graphs: Generation and application. *IEEE Transactions on Pattern Analysis and Machine Intelligence*, pages 1–1, 2021. 2

[5] Chaoqi Chen, Jiongcheng Li, Hong-Yu Zhou, Xiaoguang Han, Yue Huang, Xinghao Ding, and Yizhou Yu. Relation matters: Foreground-aware graph-based relational reasoning for domain adaptive object detection. *T-PAMI*, 2022. 1, 2

[6] Cheng Chi, Fangyun Wei, and Han Hu. Relationnet++: Bridging visual representations for object detection via transformer decoder. *Advances in Neural Information Processing Systems*, 33:13564–13574, 2020. 2

[7] Xiyang Dai, Yinpeng Chen, Bin Xiao, Dongdong Chen, Mengchen Liu, Lu Yuan, and Lei Zhang. Dynamic head: Unifying object detection heads with attentions. In *Proceedings of the IEEE/CVF Conference on Computer Vision and Pattern Recognition*, pages 7373–7382, 2021. 2

[8] Jia Deng, Nan Ding, Yangqing Jia, Andrea Frome, Kevin Murphy, Samy Bengio, Yuan Li, Hartmut Neven, and Hartwig Adam. Large-scale object classification using label relation graphs. In *European conference on computer vision*, pages 48–64. Springer, 2014. 2

[9] Jiankang Deng, Jia Guo, Niannan Xue, and Stefanos Zafeiriou. Arcface: Additive angular margin loss for deep face recognition. In *Proceedings of the IEEE/CVF conference on computer vision and pattern recognition*, pages 4690–4699, 2019. 4, 5

[10] Jiajun Deng, Yingwei Pan, Ting Yao, Wengang Zhou, Houqiang Li, and Tao Mei. Relation distillation networks for video object detection. In *Proceedings of the IEEE/CVF International Conference on Computer Vision*, pages 7023–7032, 2019. 2

[11] M. Everingham, L. Van Gool, C. K. I. Williams, J. Winn, and A. Zisserman. The pascal visual object classes (voc) challenge. *International Journal of Computer Vision*, 88(2): 303–338, 2010. 8

[12] Yuan Fang, Kingsley Kuan, Jie Lin, Cheston Tan, and Vijay Chandrasekhar. Object detection meets knowledge graphs. International Joint Conferences on Artificial Intelligence, 2017. 2

[13] Chelsea Finn, Pieter Abbeel, and Sergey Levine. Model-agnostic meta-learning for fast adaptation of deep networks. In *International conference on machine learning*, pages 1126–1135. PMLR, 2017. 2, 4

[14] Peng Gao, Minghang Zheng, Xiaogang Wang, Jifeng Dai, and Hongsheng Li. Fast convergence of detr with spatially modulated co-attention. In *Proceedings of the IEEE/CVF International Conference on Computer Vision*, pages 3621–3630, 2021. 2

[15] Ziteng Gao, Limin Wang, Bing Han, and Sheng Guo. Adamixer: A fast-converging query-based object detector. In *CVPR*, 2022. 2

[16] Chunjiang Ge, Rui Huang, Mixue Xie, Zihang Lai, Shiji Song, Shuang Li, and Gao Huang. Domain adaptation via prompt learning. *arXiv preprint arXiv:2202.06687*, 2022. 2

[17] Ross Girshick. Fast r-cnn. In *Proceedings of the IEEE international conference on computer vision*, pages 1440–1448, 2015. 1, 2

[18] Ross Girshick, Jeff Donahue, Trevor Darrell, and Jitendra Malik. Rich feature hierarchies for accurate object detection and semantic segmentation. In *Proceedings of the IEEE conference on computer vision and pattern recognition*, pages 580–587, 2014. 1, 2

[19] Kaiming He, Xiangyu Zhang, Shaoqing Ren, and Jian Sun. Deep residual learning for image recognition. In *Proceedings of the IEEE conference on computer vision and pattern recognition*, pages 770–778, 2016. 5

[20] Neil Houlsby, Andrei Giurgiu, Stanislaw Jastrzebski, Bruna Morrone, Quentin De Laroussilhe, Andrea Gesmundo, Mona Attariyan, and Sylvain Gelly. Parameter-efficient transfer learning for nlp. In *International Conference on Machine Learning*, pages 2790–2799. PMLR, 2019. 2

[21] Han Hu, Jiayuan Gu, Zheng Zhang, Jifeng Dai, and Yichen Wei. Relation networks for object detection. In *Proceedings of the IEEE conference on computer vision and pattern recognition*, pages 3588–3597, 2018. 2

[22] Xuecai Hu, Haoyuan Mu, Xiangyu Zhang, Zilei Wang, Tieniu Tan, and Jian Sun. Meta-sr: A magnification-arbitrary network for super-resolution. In *Proceedings of the IEEE/CVF conference on computer vision and pattern recognition*, pages 1575–1584, 2019. 2

[23] Menglin Jia, Luming Tang, Bor-Chun Chen, Claire Cardie, Serge Belongie, Bharath Hariharan, and Ser-Nam Lim. Visual prompt tuning. In *Computer Vision–ECCV 2022: 17th European Conference, Tel Aviv, Israel, October 23–27, 2022, Proceedings, Part XXXIII*, pages 709–727. Springer, 2022. 2

[24] Junho Kim, Inwoo Hwang, and Young Min Kim. Ev-tta: Test-time adaptation for event-based object recognition. In *Proceedings of the IEEE/CVF Conference on Computer Vision and Pattern Recognition (CVPR)*, pages 17745–17754, 2022. 2

[25] Joseph Kj, Jathushan Rajasegaran, Salman Khan, Fahad Shahbaz Khan, and Vineeth N Balasubramanian. Incremental object detection via meta-learning. *IEEE Transactions on Pattern Analysis and Machine Intelligence*, 2021. 2

[26] Feng Li, Hao Zhang, Shilong Liu, Jian Guo, Lionel M Ni, and Lei Zhang. Dn-detr: Accelerate detr training by introducing

query denoising. In *Proceedings of the IEEE/CVF Conference on Computer Vision and Pattern Recognition*, pages 13619–13627, 2022. 2

[27] Zheng Li, Xiaocong Du, and Yu Cao. Gar: Graph assisted reasoning for object detection. In *Proceedings of the IEEE/CVF Winter Conference on Applications of Computer Vision*, pages 1295–1304, 2020. 1, 2

[28] Tsung-Yi Lin, Michael Maire, Serge Belongie, James Hays, Pietro Perona, Deva Ramanan, Piotr Dollár, and C Lawrence Zitnick. Microsoft coco: Common objects in context. In *European conference on computer vision*, pages 740–755. Springer, 2014. 1, 5

[29] Tsung-Yi Lin, Priya Goyal, Ross Girshick, Kaiming He, and Piotr Dollár. Focal loss for dense object detection. In *Proceedings of the IEEE international conference on computer vision*, pages 2980–2988, 2017. 2

[30] Yutong Lin, Yuhui Yuan, Zheng Zhang, Chen Li, Nanning Zheng, and Han Hu. Detr doesn’t need multi-scale or locality design, 2023. 3

[31] Wei Liu, Dragomir Anguelov, Dumitru Erhan, Christian Szegedy, Scott Reed, Cheng-Yang Fu, and Alexander C Berg. Ssd: Single shot multibox detector. In *European conference on computer vision*, pages 21–37. Springer, 2016. 2

[32] Yong Liu, Ruiping Wang, Shiguang Shan, and Xilin Chen. Structure inference net: Object detection using scene-level context and instance-level relationships. In *Proceedings of the IEEE conference on computer vision and pattern recognition*, pages 6985–6994, 2018. 1, 2

[33] Haoyu Lu, Mingyu Ding, Yuqi Huo, Guoxing Yang, Zhiwu Lu, Masayoshi Tomizuka, and Wei Zhan. Uniadapter: Unified parameter-efficient transfer learning for cross-modal modeling. *arXiv preprint arXiv:2302.06605*, 2023. 2

[34] Shuaicheng Niu, Jiaxiang Wu, Yifan Zhang, Zhiqian Wen, Yaofu Chen, Peilin Zhao, and Mingkui Tan. Towards stable test-time adaptation in dynamic wild world. In *The Eleventh International Conference on Learning Representations*, 2023. 2

[35] Adam Paszke, Sam Gross, Francisco Massa, Adam Lerer, James Bradbury, Gregory Chanan, Trevor Killeen, Zeming Lin, Natalia Gimelshein, Luca Antiga, Alban Desmaison, Andreas Kopf, Edward Yang, Zachary DeVito, Martin Raison, Alykhan Tejani, Sasank Chilamkurthy, Benoit Steiner, Lu Fang, Junjie Bai, and Soumith Chintala. PyTorch: An Imperative Style, High-Performance Deep Learning Library. In *Advances in Neural Information Processing Systems 32*, pages 8024–8035. Curran Associates, Inc., 2019. 5

[36] Joseph Redmon, Santosh Divvala, Ross Girshick, and Ali Farhadi. You only look once: Unified, real-time object detection. In *Proceedings of the IEEE conference on computer vision and pattern recognition*, pages 779–788, 2016. 2

[37] Shaoqing Ren, Kaiming He, Ross Girshick, and Jian Sun. Faster r-cnn: Towards real-time object detection with region proposal networks. *Advances in neural information processing systems*, 28, 2015. 1, 2

[38] Byungseok Roh, JaeWoong Shin, Wuhyun Shin, and Saehoon Kim. Sparse detr: Efficient end-to-end object detection with learnable sparsity. In *ICLR*, 2022. 2

[39] Shuai Shao, Zeming Li, Tianyuan Zhang, Chao Peng, Gang Yu, Xiangyu Zhang, Jing Li, and Jian Sun. Objects365: A large-scale, high-quality dataset for object detection. In *ICCV*, 2019. 8, 17

[40] Krishna Kumar Singh, Dhruv Mahajan, Kristen Grauman, Yong Jae Lee, Matt Feiszli, and Deepti Ghadiyaram. Don’t judge an object by its context: learning to overcome contextual bias. In *Proceedings of the IEEE/CVF Conference on Computer Vision and Pattern Recognition*, pages 11070–11078, 2020. 2

[41] Leon Amadeus Varga and Andreas Zell. Tackling the background bias in sparse object detection via cropped windows. In *Proceedings of the IEEE/CVF International Conference on Computer Vision*, pages 2768–2777, 2021. 2

[42] Ashish Vaswani, Noam Shazeer, Niki Parmar, Jakob Uszkoreit, Llion Jones, Aidan N Gomez, Łukasz Kaiser, and Illia Polosukhin. Attention is all you need. *Advances in neural information processing systems*, 30, 2017. 2, 3

[43] Vibashan VS, Poojan Oza, and Vishal M. Patel. Towards online domain adaptive object detection. In *Proceedings of the IEEE/CVF Winter Conference on Applications of Computer Vision (WACV)*, pages 478–488, 2023. 2

[44] Dequan Wang, Evan Shelhamer, Shaoteng Liu, Bruno Olshausen, and Trevor Darrell. Tent: Fully test-time adaptation by entropy minimization. *arXiv preprint arXiv:2006.10726*, 2020.

[45] Qin Wang, Olga Fink, Luc Van Gool, and Dengxin Dai. Continual test-time domain adaptation. In *Proceedings of Conference on Computer Vision and Pattern Recognition*, 2022. 2

[46] Xudong Wang, Zhaowei Cai, Dashan Gao, and Nuno Vasconcelos. Towards universal object detection by domain attention. In *Proceedings of the IEEE/CVF Conference on Computer Vision and Pattern Recognition*, pages 7289–7298, 2019. 2

[47] Yu-Xiong Wang, Deva Ramanan, and Martial Hebert. Meta-learning to detect rare objects. In *Proceedings of the IEEE/CVF International Conference on Computer Vision*, pages 9925–9934, 2019. 2

[48] Kun Xia, Le Wang, Sanping Zhou, Nanning Zheng, and Wei Tang. Learning to refactor action and co-occurrence features for temporal action localization. In *Proceedings of the IEEE/CVF Conference on Computer Vision and Pattern Recognition*, pages 13884–13893, 2022. 2

[49] Hongyu Xu, Xutao Lv, Xiaoyu Wang, Zhou Ren, Navaneeth Bodla, and Rama Chellappa. Deep regionlets for object detection. In *Proceedings of the European conference on computer vision (ECCV)*, pages 798–814, 2018. 2

[50] Hang Xu, Chenhan Jiang, Xiaodan Liang, and Zhenguo Li. Spatial-aware graph relation network for large-scale object detection. In *Proceedings of the IEEE/CVF Conference on Computer Vision and Pattern Recognition*, pages 9298–9307, 2019. 2

[51] Chengxuan Ying, Tianle Cai, Shengjie Luo, Shuxin Zheng, Guolin Ke, Di He, Yanming Shen, and Tie-Yan Liu. Do transformers really perform badly for graph representation? In *Thirty-Fifth Conference on Neural Information Processing Systems*, 2021. 3

[52] Gongjie Zhang, Zhipeng Luo, Kaiwen Cui, and Shijian Lu. Meta-detr: Image-level few-shot object detection with inter-class correlation exploitation. *arXiv preprint arXiv:2103.11731*, 2021. 2

[53] Gongjie Zhang, Zhipeng Luo, Yingchen Yu, Kaiwen Cui, and Shijian Lu. Accelerating DETR convergence via semantic-aligned matching. In *Proceedings of the IEEE/CVF Conference on Computer Vision and Pattern Recognition (CVPR)*, pages 949–958, 2022. 2

[54] Hao Zhang, Feng Li, Shilong Liu, Lei Zhang, Hang Su, Jun Zhu, Lionel M Ni, and Heung-Yeung Shum. Dino: Detr with improved denoising anchor boxes for end-to-end object detection. *arXiv preprint arXiv:2203.03605*, 2022. 3, 4, 5, 6, 13, 15

[55] Xizhou Zhu, Weijie Su, Lewei Lu, Bin Li, Xiaogang Wang, and Jifeng Dai. Deformable detr: Deformable transformers for end-to-end object detection. *arXiv preprint arXiv:2010.04159*, 2020. 2, 3, 4, 5, 8, 13, 15, 16

How to calculate E_t ?

1. Assume there are 3 classes (A, B, C). All matrices will be in shape (3,3).

2. Assume we have 3 samples in training set.

They contain class [A, B, C], [B, C], [A, C], respectively.

3. Calculate conditional probabilities and fill in the matrix.

	A	B	C
A	1	0.5	0.66
B	0.5	1	0.66
C	1	1	1

4. The diagonal is always 1, because e.g., $P(A|A) = 1$.

How to calculate E_x ?

1. For instance, we want to estimate it from the single [A, C] sample.

We have $P(A|C) = 1$; $P(C|A) = 1$; $P(B|A) = 0$; $P(B|C) = 0$.

2. Use the flat prior E_0 for the rest cells as nothing is known for them.

E_x	<table border="1"> <tr> <td>1</td><td>0.5</td><td>1</td></tr> <tr> <td>0</td><td>1</td><td>0</td></tr> <tr> <td>1</td><td>0.5</td><td>1</td></tr> </table>	1	0.5	1	0	1	0	1	0.5	1	E_x	<table border="1"> <tr> <td>1</td><td>0</td><td>0</td></tr> <tr> <td>0.5</td><td>1</td><td>1</td></tr> <tr> <td>0.5</td><td>1</td><td>1</td></tr> </table>	1	0	0	0.5	1	1	0.5	1	1	E_x	<table border="1"> <tr> <td>1</td><td>1</td><td>1</td></tr> <tr> <td>1</td><td>1</td><td>1</td></tr> <tr> <td>1</td><td>1</td><td>1</td></tr> </table>	1	1	1	1	1	1	1	1	1
1	0.5	1																														
0	1	0																														
1	0.5	1																														
1	0	0																														
0.5	1	1																														
0.5	1	1																														
1	1	1																														
1	1	1																														
1	1	1																														

Sample 1: [A, C] Sample 2: [B, C] Sample 3: [A, B, C]

3. Note, the j -th column of E_t equals the average over the E_x matrices where the class j is present. For instance, the first column of E_t is the same as the average of the first column over the sample 1 and 3.

How to calculate E_b ?

The way to calculate is **identical** to that of calculating E_t . Similar to E_x , the cells corresponding to missing classes are filled with flat prior. The **only difference** is that E_t is calculated over the whole training dataset, while the batch-wise E_b is calculated over an arbitrary mini-batch.

Figure 12. Detailed demonstration on the way to calculate E_t and E_x . The calculation method is also described in footnotes in the manuscript where we introduce “Binding Detector Behavior to E ”.

A. More Technical Details & Discussions

A.1. Calculation of Matrix E

Definition. The edge $E \in [0, 1]^{K \times K}$ is a conditional probability matrix, where the (i, j) -th element is $P(i|j)$, namely the probability that “class i ” appears in an image given “the presence of class j ”. This is already made clear in the manuscript. To clearly demonstrate how the matrix E is computed, we will provide examples in Fig. 12, and reference Python code implementation to make it crystal clear.

(a). Flat Prior E_0 . Flat prior E_0 is the edge when everything is completely unknown. Assume we have K object classes, and 0 examples for calculating the $K \times K$ conditional probabilities. In this case, as nothing is known about the class i and class j , given the presence of class j , the probability of the presence of class i equals the probability of the absence of class i . Thus both probabilities are 0.5. Only when $i = j$, the $P(i|j)$ will be 1. Thus, as described in the footnotes in the manuscript, E_0 is a symmetric matrix, where its diagonal values are 1, and all the off-diagonal

values are 0.5:

$$E_0 = \begin{bmatrix} 1 & 0.5 & 0.5 & \cdots & 0.5 \\ 0.5 & 1 & \ddots & \ddots & \vdots \\ 0.5 & \ddots & \ddots & \ddots & 0.5 \\ \vdots & \ddots & \ddots & 1 & 0.5 \\ 0.5 & \cdots & 0.5 & 0.5 & 1 \end{bmatrix}.$$

Based on the flat prior, if the probability $P(i|j) < 0.5$, it can be interpreted as “class i is less likely to appear given the presence of class j ”, and there is already some information about class i and j . Likewise, if the probability $P(i|j) > 0.5$, it can be interpreted as “class i is more likely to appear given the presence of class j ”.

Example Python code for E_0 :

```
import numpy as np

def edge_flat_prior(num_cls: int) -> np.ndarray:
    E = np.ones((num_cls, num_cls)) * 0.5
    np.fill_diagonal(E, 1.0)
    return E

print(edge_flat_prior(5))
```

(b). Calculation of E_t , E_v , E_b , and E_x . The only difference among them is the number of samples used to calculate the statistics (conditional probability). Specifically, E_t is calculated on the whole COCO training set. The E_v is calculated on the whole COCO validation set. The E_b is dynamically calculated on an arbitrary given mini-batch during the training or inference stage. The E_x is dynamically calculated for a single image during the training or inference stage. The notation $E_{b(2)}$, for instance, means the E_b calculated on a two-image mini-batch. By definition, E_t is equivalent to E_b by treating the whole training dataset as a mini-batch. Note, following the idea of flat prior E_0 , when the class j does not exist in the population at all, we use the corresponding value in the flat prior.

Recall that $P(i|j) = P(i, j)/P(j)$. Therefore, the calculation is to count the co-occurrence of (i, j) classes, and then divide it by the occurrence count of class j . See Fig. 12 for detailed examples.

We also use \overline{E}_x in the manuscript, which is a “flipped” version of E_x . This provides a “misleading” deployment prior for testing our model as a sanity check for whether the model behavior follows the input E . The calculation is identical to E_x , except for that we fill 1 in the matrix where $P(i|j) = 0$, and 0 where $P(i|j) = 1$, and the the diagonal is left intact.

Example Python code for E_x :

```
from typing import *
import numpy as np

sample1 = [0, 2] # contains A, C
sample2 = [1, 2] # contains B, C
```

```
sample3 = [0, 1, 2] # contains A, B, C

def edge_sample(num_cls: int,
               labels: List[int]) -> np.ndarray:
    E = np.ones((num_cls, num_cls)) * 0.5
    for j in labels:
        E[:, j] = 0.0
        E[j, :] = 1.0
    np.fill_diagonal(E, 1.0)
    return E

print(edge_sample(3, sample1))
print(edge_sample(3, sample2))
print(edge_sample(3, sample3))
```

Example Python code for E_b :

```
from typing import *
import numpy as np
import itertools as it

sample1 = [0, 2] # contains A, C
sample2 = [1, 2] # contains B, C
sample3 = [0, 1, 2] # contains A, B, C

def sparse2dense(num_cls: int,
                 targets: List[List[int]]) -> np.ndarray:
    dense = np.zeros((num_cls, len(targets)))
    for (j, labels) in enumerate(targets):
        dense[labels, j] = 1.0
    return dense

def dense2edge(dense: np.array) -> np.ndarray:
    num_cls, batch_size = dense.shape
    E = np.ones((num_cls, num_cls)) * 0.5
    rN = range(num_cls)
    for (i, j) in it.product(rN, rN):
        cij = np.logical_and(dense[i, :], dense[j, :]).sum()
        cj = dense[j, :].sum()
        if cj > 0:
            pij = cij / cj
        else:
            pij = 0.5 # flat prior
        E[i, j] = pij
    np.fill_diagonal(E, 1.0)
    return E

def edge_batch(num_cls: int,
              targets: List[List[int]]) -> np.ndarray:
    dense = sparse2dense(num_cls, targets)
    E = dense2edge(dense)
    return E

batch = [sample1, sample2, sample3]
print(edge_batch(3, batch))
```

The Python code for E_t is completely identical to E_b by treating the whole COCO training set as a single batch. Note, the above Python code snippets are only for demonstration. Our actual implementation is optimized using Cython.

A.2. Regarding Graph $\langle V, E \rangle$

(a). Conditional Probability. The extent that class j depends on class i does not necessarily equal the extent that the class i depends on class j . The edge should be directional (asymmetric). Since conditional probability is asymmetric, it can indicate the relation in a directional way. In contrast, symmetric relations, such as co-occurrence probability and correlation are not suitable here.

(b). Implicitly Learned Edge. Learning the edges implicitly, without a clear definition for its entries, could make the interpretation of model behavior and self-calibration difficult. In this paper, we use manually selected conditional probability for describing the characteristics of distribution and its shift for interpretability. Implicitly learned distribution characteristics are left for future study.

(c). Columns of E . The j -th column are the conditional probabilities that the class i appears given the presence of j . If $P(i|j) = 1.0$, it means class i always appears together with j . As a result, the model learns the representation of class j with the information from class i entangled. If $P(i|j) = 0.0$, the representation of class j will suppress the information from class i . The j -th column vector of E represents exactly how each class i contributes to the representation of class j . Using the j -th row for class j is incorrect by design.

(d). Calibration of nodes V . As explained in the manuscript, the calibration of nodes V is conceptually incremental or transfer learning, which is beyond the scope of this paper. See Fig. 13 for the demonstration. We leave this as a direction for future study.

(e). Underlying Idea. The core idea of CaliDet can be isolated from the object detection task. Assuming that some statistical properties of the test distribution can be characterized, we may be able to bind the model behavior with such properties as an input, and calibrate the model at the run-time for the distribution shift without any change to the model parameter. This problem setting is even more challenging than test-time adaptation, but more efficient in terms of computation cost. In particular, the “statistical property” used in this paper is object relation, namely the conditional probability between two object classes. If we regard such object relation as second-order information, we can consider using different statistical properties in other tasks. For instance, in long-tail image classification, we may leverage the class distribution, which is first-order information. We leave these possibilities for future study.

A.3. Model Design and Training

A.3.1 CaliFormer and Prediction Head

(a). Model Capacity. The default number of layers of CaliFormer is 3. When the number of layers is decreased from 3 to 1, the capacity of CaliFormer is insufficient for

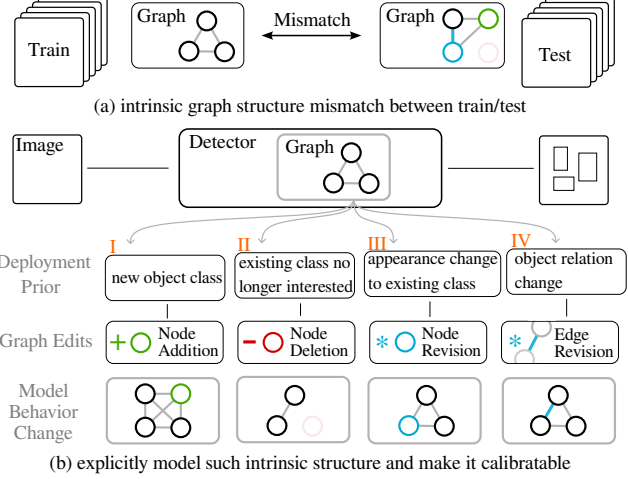


Figure 13. Calibration of both nodes V and edges E is a more complicated and challenging issue. The node addition, node deletion, and node revision are conceptually incremental learning or transfer learning. Our current model only implements the fourth type of deployment prior injection, namely the edge revision, because this is uncharted in the literature. The other three types of graph edits are widely explored for object detection. Combining all of these types of graph edits could be one of the future research directions.

the model to generalize against different edges will decrease. When the number of layers is increased to more than 3, the performance gain through injection turns to be marginal.

(b). ΔE and flat prior E_0 . The difference ΔE is designed to represent the extent of change for the dependency of one class to another class, compared to the case where nothing is known. We should not calculate ΔE as $E - E_t$, because E_t is already biased towards the training set. Only the flat prior can present “nothing is known”.

(c). Scaling Factor ρ . This hyper-parameter should not be too large. A large ρ such as 1.0 makes the classification layer excessively distracted to harm the classification accuracy. We empirically set it as 0.2 based on our observations.

(d). Decoder Layers. The detector involves 6 layers of Decoders. Each layer of the decoder has its own classification heads and an auxiliary loss. We share the same CaliFormer among all the prediction heads for all 6 decoder layers.

(e). Compatibility. CaliDet is not coupled with any particular DETR-like detector, and can be incorporated into other DETR-like models. It only contains three core components: (1) calibration vector; (2) LoMa loss; (3) edge sampling distribution. This document includes results of CaliDet based on D-DETR [55] instead of DINO [54]. We leave the one-stage and two-stage detectors for future study.

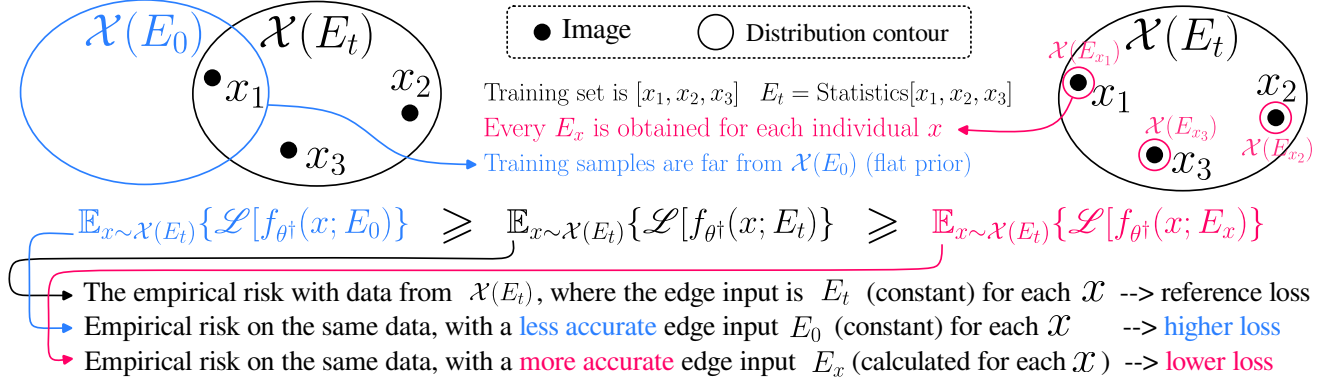


Figure 14. Illustration of Eq. 5 in the manuscript.

A.3.2 Logit Matching Loss (LoMA)

The LoMa loss term is proposed in order to make the loss landscape vary based on the values of the input matrix E . Without it, the loss landscape is invariant to the input E , and cannot properly and effectively guide the model towards the correct usage of information in E . It is designed to indirectly enforce Eq. 5 in the manuscript. The illustration of Eq. 5 can be found in Fig. 14.

Without the LoMA loss function, the model fails to generalize and satisfy the expected order of AP given different E . This is because the model lacks an explicit penalty to learn to leverage the information in E . The LoMA loss weight γ can be adjusted. We empirically set it as 20 for both DINO and D-DETR variants of CaliDet for the best results.

A.3.3 Edge Sampling Distribution

(a). When no $\{E_t\}$ in \mathcal{E} . If the E_t is removed, the model will not generalize well around E_t , as $AP(E_t)$ is lower than $AP(E_0)$, failing the sanity test on the expected AP order.

(b). When only $\{E_x\}$ in \mathcal{E} . This leads to very poor generalization around E_t . Namely the $AP(E_t)$ is much lower than $AP(E_0)$, which fails the sanity test. Diversity is needed in the sampling distribution. Results are omitted.

(c). When no Gaussian noise in \mathcal{E} . This leads to poor generalization and fails to satisfy the expected order of AP. Namely, the $AP(E_v)$ is slightly lower than $AP(E_t)$, which indicates the failure of generalization against different priors. Noise is necessary.

(d). Magnitude of Gaussian Noise. A slightly smaller Gaussian noise leads to a larger gap between $AP(E_t)$ and $AP(E_0)$, but a smaller gap between $AP(E_t)$ and $AP(E_v)$. A too small Gaussian noise will result in overfitting to the constant edges such as E_t , and fail to generalize against different priors. In contrast, if the Gaussian noise is too large, the model will gradually lose the sensitivity against

the injected prior, due to the information being too noisy. We empirically select the Gaussian parameter as $\mathcal{N}(0, 0.16^2)$ for best generalization.

(e). Parameter Tuning. One important clue to observe during hyper-parameter tuning is to make sure that E_v performance is slightly higher than E_t – only in this way can the model correctly generalize against new conditional probability shifts. When adapting CaliDet to a new model with a different training batch size, the other edges such as $E_{b(4)}$ (statistics on 4-sample mini-batch) can be added to the edge sampling algorithm to increase edge diversity during training. For instance, this is done in the CaliDet (D-DETR) experiments in this supplementary document.

A.4 Inference & Self-Calibration

(a). Run-time Calibration. During the inference stage, the model architecture, as well as the parameters of CaliDet is completely frozen. The back-propagation is not allowed in the “run-time calibration” setting. See Section A.4.1 for the discussion on the advantages of a run-time calibration. The calibration (i.e., deployment prior injection) process is done by simply changing the input matrix E . Note, our calibratable detector accepts an additional input E besides the image.

(b). Cached V' . If the input E is a fixed constant, we can cache the calculated calibration vector $V' = g(V, \Delta E)$, and reduce the CaliFormer overhead to nearly zero, depending on the update frequency of E . In this case the only computational overhead is the matrix addition operation: $W + \rho V'$. In practice, the deployment prior does not have to be changed upon every forward pass. Instead, the deployment prior can be updated periodically, for instance once per hour. Thus, as long as E does not frequently change, the computation cost of run-time calibration can be reduced to nearly zero by such an engineering technique to cache the calibration vectors. And the inference cost will solely depend on the baseline

detector itself when the deployment prior is not changed.

(c). Initialization with E_t . Our self-calibration process is initialized as $E_c \leftarrow E_t$, inheriting the training set prior. This means that we assume the test distribution is close to the training set when nothing is known about the test set at the beginning of self-calibration. If the algorithm is initialized with E_0 , the AP will be lower than $AP(E_t)$. Thus, we empirically initialize E_c from the default prior E_t .

A.4.1 Advantage of Run-Time Calibration

(1). If a calibratable detector is used on hundreds of edge devices, they can be calibrated toward their local distribution shifts. The calibration process is merely changing the $K \times K$ input matrix E without any change to the network architecture or the parameters. That means the calibration process can be done by weak devices locally. Compared to existing works that adapt a detector and involve back-propagation, fine-tuning a detector for hundreds of devices with some new data is still not a negligible cost, which is repetitive and much more costly than run-time calibration.

(2). Through the self-calibration process, CaliDet can calibrate itself towards the test data distribution without human annotation. Since the default $AP(E_t)$ of CaliDet is on par with the baseline detector, it is usable as a drop-in replacement for a general detector. Thus, designing a run-time calibratable detector is very challenging.

The core underlying idea of CaliDet is in fact independent to object detection. Assume a training dataset has some physically interpretable bias that can be described by a set of parameters. Presumably, a deep model well-learned on such a dataset will also inherit such bias. Such bias can be either harmful or helpful depending on the proximity of the test distribution and the training distribution. If we supplement the physically meaningful parameters directly to the model input, and let the model understand what these parameters mean, we should be able to adapt the model towards the distribution shift with respect to the mentioned parameters by merely changing the input parameters.

This work can also be seen as extending the object detector to be promptable, where the format of such “prompt” is fixed as the conditional probability matrix E . We hope this work could inspire readers beyond the area of object detection. For instance, can we consider other types of human-understandable training set characteristics, and design more controllable deep network models with run-time calibration capability?

A.5. Visualization of Self-Calibration

We provide some visualization results for the self-calibration algorithm. We filter out the detection results with a score less than 0.5. For self-calibration results on subsets of size 256, some results can be found in Fig. 15 and Fig. 16. For

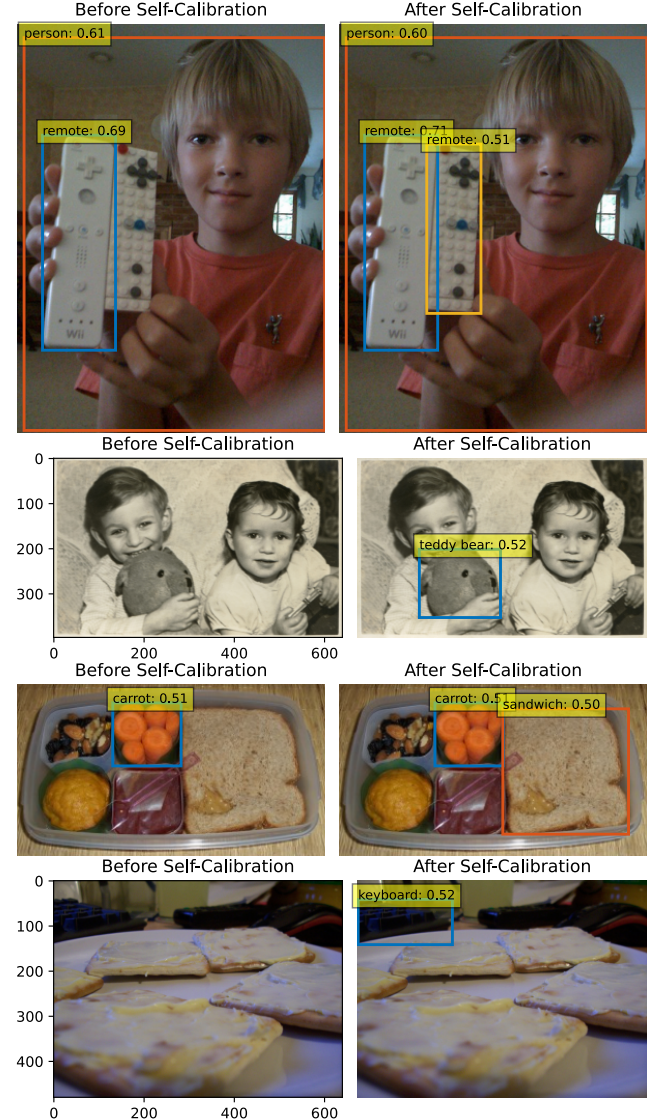


Figure 15. Visualization of Self-Calibration with CaliDet (DINO). The corresponding subset size is 256. (Part 1 of 2)

self-calibration results on subsets of size 8, some results can be found in Fig. 17. As can be seen from the figures, after deployment prior injection or self-calibration, the model’s confidence will increase, and hence, some missed detections will appear after calibration. Self-calibration is effective.

B. Porting to D-DETR [55]

In this subsection, we implement our proposed method onto Deformable-DETR [55] (abbr., D-DETR), which is also commonly referred to as one of the state-of-the-art method in the recent detection literature besides DINO [54]. We adopt the single-scale variant of D-DETR as the base model. According to the following experiments, our method is effective on

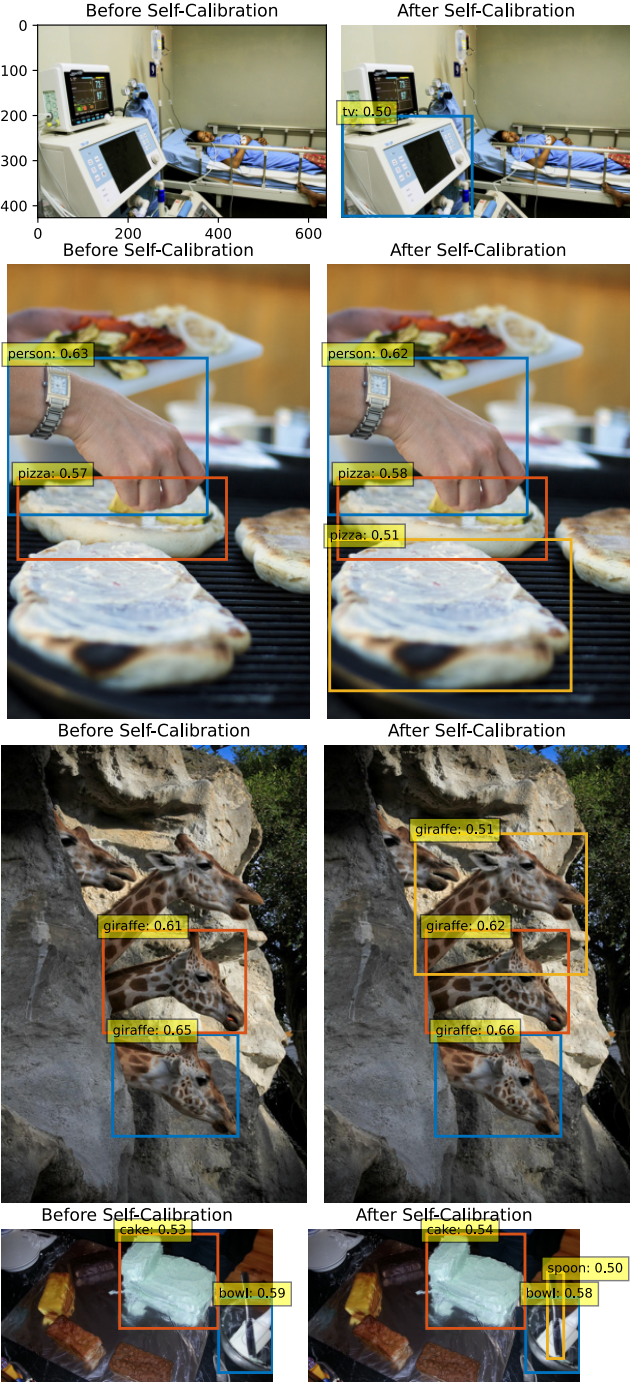


Figure 16. Visualization of Self-Calibration with CaliDet (DINO). The corresponding subset size is 256. (Part 2 of 2)

D-DETR.

B.1. Experimental Setup and Results

There are three parts of evaluations. (1) The standard COCO evaluation results can be found in Tab. 4. (2) The subset

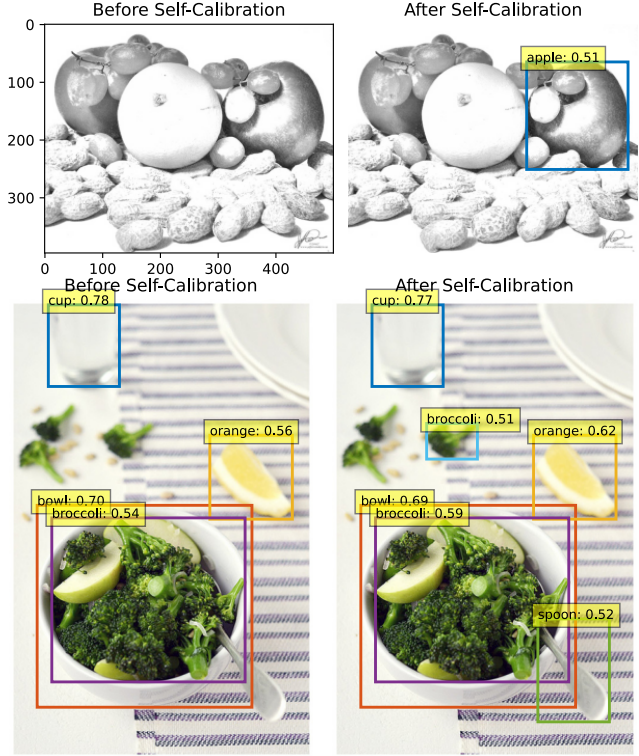


Figure 17. Visualization of Self-Calibration with CaliDet (DINO). The corresponding subset size is 8.

Method	Injection	Standard COCO Metrics					
		AP	AP ₅₀	AP ₇₅	AP _S	AP _M	AP _L
D-DETR	-	41.47	61.87	44.73	24.18	45.30	55.95
	E_x	36.38	51.95	39.77	18.53	39.92	51.72
	E_0	41.49	60.78	44.96	23.52	45.41	56.17
	E_t	41.69	61.82	45.02	23.52	45.42	56.39
(D-DETR)	E_v	41.70	61.84	45.03	23.52	45.43	56.41
	E_b	43.66	65.17	46.69	25.59	47.34	58.15
	E_x	43.92	65.61	47.22	25.68	47.55	58.85

Table 4. Standard COCO Evaluation Results. We incorporate our proposed CaliDet method to the D-DETR [55] model (single scale variant). The results suggest that our method is effective on D-DETR, as the performance order given different deployment priors is as expected.

evaluations can be found in Tab. 5. (3) The self-calibration results for varying subset sizes can be found in Fig. 18, Fig. 19, Fig. 20, Fig. 21, Fig. 22, and Fig. 23. All these results show that CaliDet is effective on the D-DETR model. We conclude that CaliDet is not coupled with DINO, and we speculate that CaliDet should be effective on other DETR-like models.

Subset Size	Injection	ϵ	COCO Metrics Averaged over Subsets					
			AP	AP ₅₀	AP ₇₅	AP _S	AP _M	AP _L
8	E_t	0	55.35	75.34	59.72	34.91	58.79	73.96
	$E_{b(8)}$	0.331	55.64	75.80	60.00	35.18	59.02	74.32
16	E_t	0	53.64	73.31	57.80	33.50	57.23	72.35
	$E_{b(16)}$	0.276	53.85	73.66	57.98	33.65	57.36	72.56
32	E_t	0	52.30	71.61	56.38	32.16	55.76	70.75
	$E_{b(32)}$	0.202	52.48	71.85	56.56	32.31	55.88	70.91
64	E_t	0	50.54	69.76	54.54	31.02	54.51	68.71
	$E_{b(64)}$	0.122	50.70	69.99	54.69	31.08	54.55	68.83
128	E_t	0	48.36	67.57	52.18	29.97	52.75	66.40
	$E_{b(128)}$	0.062	48.48	67.71	52.31	30.03	52.77	66.49
256	E_t	0	46.21	65.62	49.77	28.78	50.60	63.93
	$E_{b(256)}$	0.034	46.31	65.76	49.86	28.78	50.64	63.95

Table 5. Subset Evaluation with Varying Subset Size. This experiment is based on D-DETR and COCO dataset. We split all validation data to subsets with different sizes. This means with a frozen, we can still obtain some AP improvements for free (*i.e.*, without any gradient update) given an arbitrary distribution shift in terms of the conditional probability.

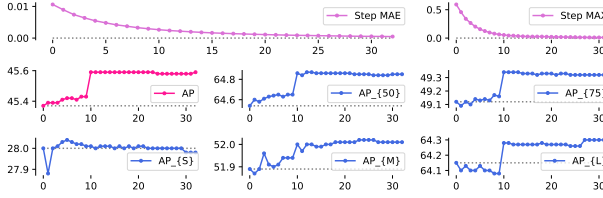


Figure 18. Self-calibration results on COCO dataset using CaliDet (D-DETR) w/ subset size 256.

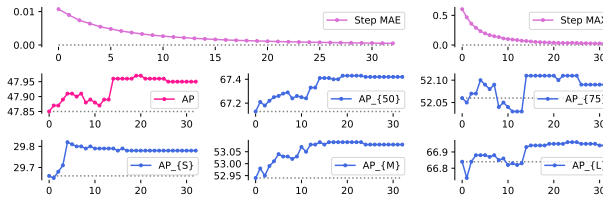


Figure 19. Self-calibration results on COCO dataset using CaliDet (D-DETR) w/ subset size 128.

B.2. Visualization of Self-Calibration

We provide some visualization results for the self-calibration algorithm. We filter out the detection results with a score of less than 0.5. For self-calibration results on subsets of size 256, some results can be found in Fig. 24. As can be seen from the figures, after deployment prior injection or

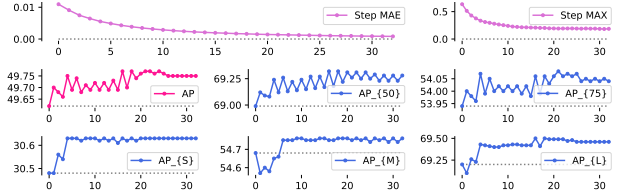


Figure 20. Self-calibration results on COCO dataset using CaliDet (D-DETR) w/ subset size 64.

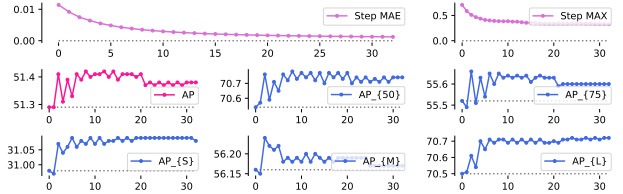


Figure 21. Self-calibration results on COCO dataset using CaliDet (D-DETR) w/ subset size 32.

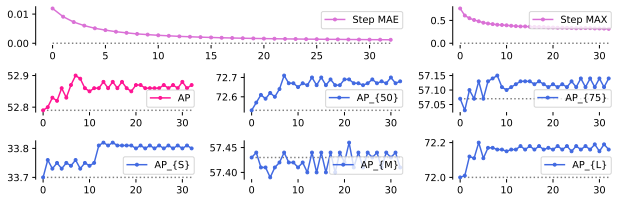


Figure 22. Self-calibration results on COCO dataset using CaliDet (D-DETR) w/ subset size 16.

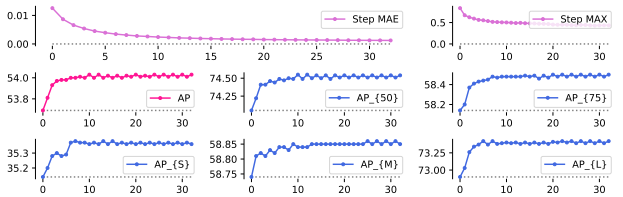


Figure 23. Self-calibration results on COCO dataset using CaliDet (D-DETR) w/ subset size 8.

self-calibration, the model’s confidence will increase, and hence some missed detections will appear after calibration.

C. Objects365 Evaluation

Objects365 [39] (O365) from ICCV2019 is a dataset designed to spur object detection research with a focus on diverse objects in the Wild. It involves 365 categories, 2 million images, and 30 million bounding boxes, which is more challenging than the COCO 2017 detection dataset.

In this section, we first freeze the CaliDet trained on the COCO training set (it has not seen any O365 training sam-

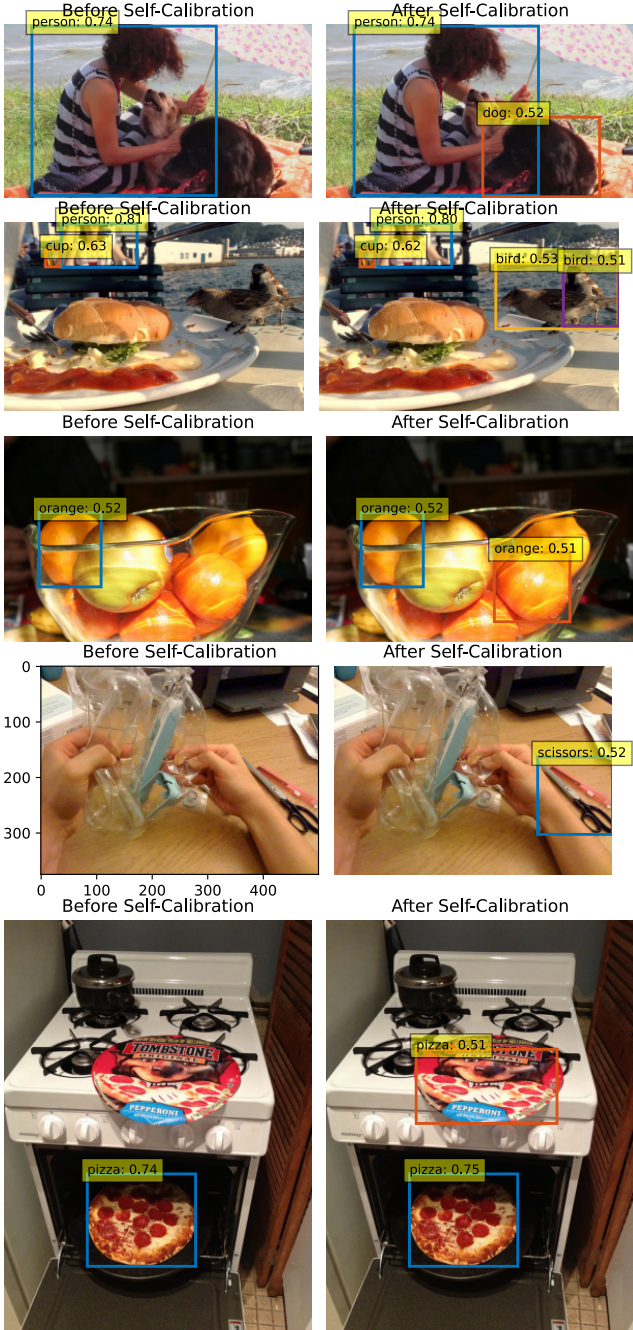


Figure 24. Visualization of Self-Calibration with CaliDet (D-DETR). The corresponding subset size is 256.

ple). Then we directly evaluate CaliDet on the Objects365 validation set without any change in the model architecture, or the parameters. Namely, the original classification heads are kept and used without any fine-tuning.

Similar to the COCO evaluations in the manuscript, we will show the standard evaluations on the O365 validation set, the O365 validation subset evaluation, as well as self-

COCO Class (in JSON format)	Objects365 Class (in JSON format)
<code>{'name': 'Wild Bird', 'id': 57}</code>	<code>{'name': 'Pigeon', 'id': 165}</code>
<code>{'id': 16, 'name': 'bird'}</code>	<code>{'name': 'Pigeon', 'id': 165}</code>
<code>{'name': 'Pigeon', 'id': 165}</code>	<code>{'name': 'Farrot', 'id': 320}</code>
<code>{'id': 31, 'name': 'handbag'}</code>	<code>{'name': 'Handbag/Satchel', 'id': 14}</code>
<code>{'id': 33, 'name': 'suitcase'}</code>	<code>{'name': 'Luggage', 'id': 121}</code>
<code>{'id': 35, 'name': 'skis'}</code>	<code>{'name': 'Skiboard', 'id': 120}</code>
<code>{'name': 'Soccer', 'id': 119}</code>	<code>{'name': 'Soccer', 'id': 119}</code>
<code>{'name': 'Other Balls', 'id': 157}</code>	<code>{'name': 'Other Balls', 'id': 157}</code>
<code>{'name': 'Baseball', 'id': 166}</code>	<code>{'name': 'Baseball', 'id': 166}</code>
<code>{'id': 37, 'name': 'sports ball'}</code>	<code>{'name': 'Basketball', 'id': 178}</code>
<code>{'name': 'Basketball', 'id': 178}</code>	<code>{'name': 'Billards', 'id': 190}</code>
<code>{'name': 'Billards', 'id': 190}</code>	<code>{'name': 'American Football', 'id': 207}</code>
<code>{'name': 'American Football', 'id': 207}</code>	<code>{'name': 'Tennis', 'id': 211}</code>
<code>{'name': 'Tennis', 'id': 211}</code>	<code>{'name': 'Volleyball', 'id': 240}</code>
<code>{'name': 'Volleyball', 'id': 240}</code>	<code>{'name': 'Golf Ball', 'id': 248}</code>
<code>{'name': 'Golf Ball', 'id': 248}</code>	<code>{'name': 'Table Tennis', 'id': 365}</code>
<code>{'id': 51, 'name': 'bowl'}</code>	<code>{'name': 'Bowl/Basin', 'id': 27}</code>
<code>{'id': 55, 'name': 'orange'}</code>	<code>{'name': 'Orange/Tangerine', 'id': 105}</code>
<code>{'id': 67, 'name': 'dining table'}</code>	<code>{'name': 'Dinning Table', 'id': 99}</code>
<code>{'id': 72, 'name': 'tv'}</code>	<code>{'name': 'Monitor/TV', 'id': 38}</code>
<code>{'id': 88, 'name': 'teddy bear'}</code>	<code>{'name': 'Stuffed Toy', 'id': 71}</code>
<code>{'id': 89, 'name': 'hair drier'}</code>	<code>{'name': 'Hair Dryer', 'id': 329}</code>

Table 6. Class Mapping between COCO Dataset and Objects365 Dataset. We build this mapping in order to directly evaluate the CaliDet (trained solely on COCO training set) on the O365 validation set. The mapping for unmentioned classes can be automatically built using case-insensitive matching in category names. Here are some details regarding the mapping: (1) We manually confirmed the “suitcase” (COCO) and the “Luggage” (O365) correspondence by examples; (2) Most “sports balls” in COCO are baseball and tennis; (3) “Dinning Table” is a typo in O365; (4) O365 contains more types of stuffed toys than “Teddy bear”.

calibration on O365 subsets.

C.1. Dataset Preprocessing

The COCO involves 80 object categories, while O365 involves 365 categories. Before the experiments, we first trim the O365 validation set and remap the classes to COCO classes, because it is impossible to use a frozen COCO model to detect the non-overlapping categories in O365.

We first manually build a class mapping between COCO and O365. Most of the 80 categories can match with a class in O365 with case-insensitive matching with their names. For all mismatching classes, we manually check example images, and build the mappings as shown in Tab. 6.

Then we filter the O365 annotations that do not associate with any COCO class, as well as the O365 images that contain zero COCO object category. The original O365 validation dataset contains 80,000 images, and 1,240,587 annotations. After removing the non-COCO classes, 71,316 images (89.1%) and 438,215 (35.2%) annotations remain.

In the end, we map the object categories in the remaining data and annotations back to the COCO category IDs. The evaluations in this section are based on this processed O365 validation set. The O365 validation set conditional probability E_v^{O365} , as well as its difference with respect to E_v^{COCO} and E_t^{COCO} can be found in Fig. 25 and Fig. 26. Note, the COCO validation statistics E_v^{COCO} deviates from E_v^{O365} fur-

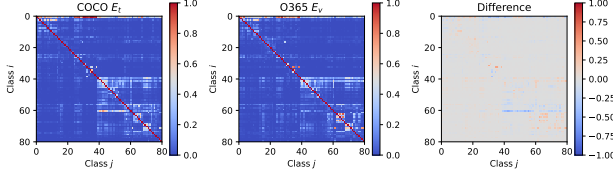


Figure 25. Comparison between E_t^{COCO} and E_v^{O365} . The MAE between them is 0.018. The max and min absolute differences are 0.526 and 0.0, respectively. The 50-, 90-, 97-th percentile values are 0.004, 0.048, and 0.122, respectively.

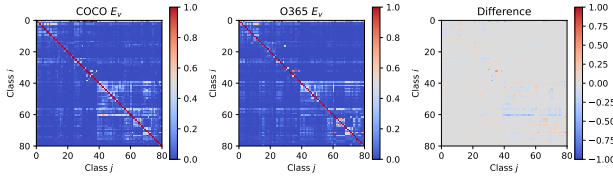


Figure 26. Comparison between E_v^{COCO} and E_v^{O365} . The MAE between them is 0.020. The max and min absolute differences are 0.506 and 0.0, respectively. The 50-, 90-, 97-th percentile values are 0.005, 0.054, and 0.132, respectively. Note, the COCO validation statistics E_v^{COCO} deviates from E_v^{O365} further than the COCO training set statistics E_t^{COCO} . Thus, the AP on O365 when we inject E_v^{COCO} should be slightly lower than E_t^{COCO} , because the former one has a larger discrepancy compared to the ground-truth E_v^{O365} .

Method	Injection	Standard Metrics on O365					
		AP	AP ₅₀	AP ₇₅	AP _S	AP _M	AP _L
CaliDet (DINO)	\overline{E}_x	24.17	31.16	26.17	7.64	20.17	38.33
	E_0	32.80	43.15	35.51	12.98	29.50	47.01
	E_t^{COCO}	33.10	43.72	35.82	13.16	29.78	47.06
	E_v^{COCO}	33.08	43.69	35.80	13.16	29.76	47.03
	E_v^{O365}	33.15	43.79	35.88	13.20	29.82	47.11
	E_b	38.80	51.82	41.98	16.94	35.69	52.83
	E_x	39.18	52.34	42.40	17.29	36.05	53.24

Table 7. Standard Detection Metrics on Objects365 (O365) Dataset. $\text{MAE}(E_t^{\text{COCO}}, E_v^{\text{O365}})=0.018$. $\text{MAE}(E_v^{\text{COCO}}, E_v^{\text{O365}})=0.020$. Our model is effective. The AP on O365 when we inject E_v^{COCO} is slightly lower than E_t^{COCO} , because the former one has a larger discrepancy compared to the ground-truth E_v^{O365} (marked in yellow).

ther than the COCO training set statistics E_t^{COCO} . Thus, the AP on O365 when we inject E_v^{COCO} should be slightly lower than E_t^{COCO} , because the former one has a larger discrepancy compared to the ground truth E_v^{O365} .

C.2. Experimental Results

We first evaluate the COCO model from the manuscript (*i.e.*, based on DINO). As shown in Tab. 7, our model is effective. Specifically, although E_v^{O365} deviates from E_t^{COCO} , most of its conditional probabilities are still roughly correct. The

Subset Size	Injection	ϵ	Metrics Averaged over O365 Subsets					
			AP	AP ₅₀	AP ₇₅	AP _S	AP _M	AP _L
8	E_t	0	55.27	68.56	58.93	32.94	54.94	72.39
	$E_b(8)$	0.336	55.62	69.04	59.30	33.35	55.26	72.57
16	E_t	0	52.29	65.08	55.79	32.80	52.39	69.61
	$E_b(16)$	0.292	52.67	65.56	56.19	33.13	52.70	69.82
32	E_t	0	49.19	61.44	52.52	30.41	49.46	66.52
	$E_b(32)$	0.235	49.57	61.92	52.92	30.68	49.75	66.73
64	E_t	0	45.84	57.54	48.97	27.73	46.16	63.22
	$E_b(64)$	0.174	46.20	58.01	49.37	27.96	46.44	63.45
128	E_t	0	42.85	54.18	45.84	25.04	42.94	59.78
	$E_b(128)$	0.120	43.14	54.55	46.16	25.20	43.15	59.99
256	E_t	0	40.42	51.48	43.33	22.57	39.96	56.83
	$E_b(256)$	0.078	40.63	51.76	43.57	22.67	40.15	57.01

Table 8. Subset Evaluation with Varying Subset Size. The CaliDet (DINO) is evaluated on Objects365 subsets. Subset Evaluation with Varying Subset Size. We split the whole validation dataset into subsets of varying sizes. With a frozen model, we can still obtain some AP improvements for free (*i.e.*, without any gradient update) given an arbitrary distribution shift in terms of the conditional probability.

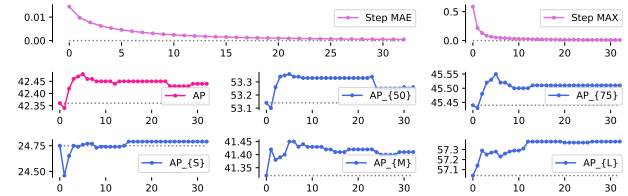


Figure 27. Self-calibration results on O365 dataset using CaliDet (DINO) w/ subset size 256.

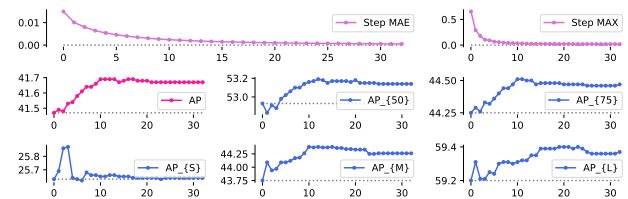


Figure 28. Self-calibration results on O365 dataset using CaliDet (DINO) w/ subset size 128.

subset evaluation result can be found in Tab. 8. The self-calibration results can be found in Fig. 27, 28, 29, 30, 31, 32.

The proposed CaliDet is effective, even if it is only trained on the COCO training set (not seen any O365 sample during training). With different deployment priors, the correspond-

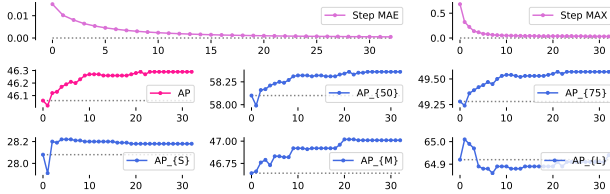


Figure 29. Self-calibration results on O365 dataset using CaliDet (DINO) w/ subset size 64.

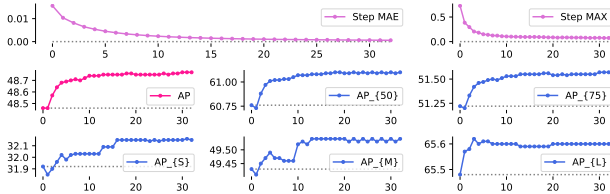


Figure 30. Self-calibration results on O365 dataset using CaliDet (DINO) w/ subset size 32.

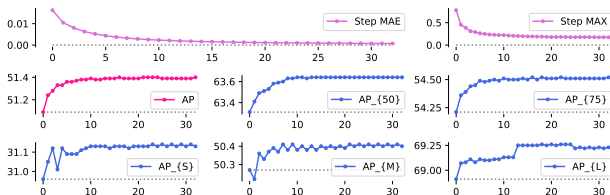


Figure 31. Self-calibration results on O365 dataset using CaliDet (DINO) w/ subset size 16.

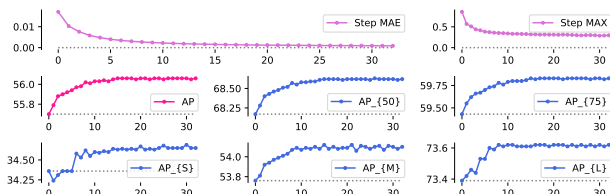


Figure 32. Self-calibration results on O365 dataset using CaliDet (DINO) w/ subset size 8.

ing AP varies following the expectation.

Apart from these, we are sorry for not having enough computational resource to provide experimental results for the full Object365 dataset (trained with all the 365 classes), or the LVIS dataset (with 1203 classes), because they require large-scale pre-training to reach a sensible AP performance. During the training process, our method requires a mostly correct matching in the decoder part to learn the correct calibration vectors on the corresponding classification heads. If the baseline model AP is low (for instance, an LVIS model without large-scale pretraining), the calibration vector learn-

ing process will be very noisy, and hence leads to a very weak calibration effect.